






Cite this: DOI: 10.1039/d5nh00138b

# Next-generation CO<sub>2</sub> electroreduction: the role of atomically precise nanoclusters and emerging catalytic strategies

Mandira Ghosh, Rupa Sarma, Maho Kamiyama, Tokuhisa Kawawaki,   
 Sourav Biswas \* and Yuichi Negishi \*

The electrochemical reduction of carbon dioxide (CO<sub>2</sub>) is a promising approach to simultaneously mitigate greenhouse gas emissions and produce value-added carbon-based fuels and chemicals. However, sluggish reaction kinetics necessitate the development of efficient catalysts to enhance activity and selectivity. Metal nanoclusters (NCs) have emerged as highly promising candidates due to their atomically precise structures, unique electronic properties, and tunable catalytic behaviors. Despite continuous advancements in the synthesis and application of metal NCs, several challenges remain that hinder their practical deployment. Stability, scalability, and the fine control of selectivity remain critical concerns. This review systematically explores the stepwise evolution of metal NCs as catalysts for CO<sub>2</sub> electroreduction, highlighting their key advantages while also identifying the fundamental limitations that need to be addressed. To overcome such challenges a key development is observed that leads to shift from noble-metal NCs to first-row transition-metal-based NCs, which has expanded catalytic reactivity and product selectivity. Additionally, the role of alloying in enhancing catalytic performance through synergistic interactions and electronic modifications is discussed. So, this review provides a comprehensive analysis of recent progress, with a focus on emerging NC-based electrocatalysts, and outlines future directions to address existing challenges for sustainable CO<sub>2</sub> conversion.

Received 10th March 2025,  
 Accepted 10th April 2025

DOI: 10.1039/d5nh00138b

rsc.li/nanoscale-horizons

## 1. Introduction

One of the most pressing challenges of environmental degradation today is the global climate crisis, exacerbated by the accelerating

depletion of fossil fuel resources. Among the various greenhouse gases contributing to global warming, carbon dioxide (CO<sub>2</sub>) is the most significant, with its atmospheric concentration reaching alarming levels.<sup>1–3</sup> The rapid industrial expansion over recent

*Institute of Multidisciplinary Research for Advanced Materials, Tohoku University, Katahira 2-1-1, Aoba-ku, Sendai 980-8577, Japan. E-mail: Sourav.biswas210@gmail.com, yuichi.negishi.a8@tohoku.ac.jp*



**Mandira Ghosh**

*Mandira Ghosh is a PhD student in in Prof. Negishi's group at Tohoku University, Japan. She received her Master's in Chemistry from National Institute of Technology Durgapur (2022). Afterward she joined at Vellore Institute of Technology, Chennai (2023) as Junior Research Fellow. Her current research focuses on the synthesis of different Cu nanocluster for the electrocatalytic CO<sub>2</sub> reduction reaction.*



**Rupa Sarma**

*Rupa Sarma is a PhD researcher in Prof. Negishi's group at Tohoku University, Japan. She obtained her Master's degree in Chemistry from National Institute of Technology Durgapur, India (2022). Her research focuses on synthesizing Cu nanoclusters, analysing their crystal structures, and exploring catalytic applications.*



decades, coupled with the continuous combustion of fossil fuels, has been a primary driver of escalating CO<sub>2</sub> emissions.<sup>4</sup> According to projections from the U.S. energy information administration, global CO<sub>2</sub> emissions are expected to rise by approximately 34% by 2050 compared to 2022 levels, posing a severe threat to climate stability.<sup>5</sup> In response to this crisis, the 29th United Nations climate change conference (COP29), held in Baku, Azerbaijan, underscored the necessity of financial support for the implementation of the Paris Agreement's long-term climate strategy.<sup>6</sup>

A central goal of this framework is to achieve carbon neutrality by 2050, necessitating a drastic reduction in net CO<sub>2</sub> emissions. Meanwhile, the global energy sector is undergoing a transformative shift towards sustainable alternatives, including solar, wind, and hydropower, to reduce dependence on finite fossil fuel reserves and address the soaring global energy demand.<sup>7,8</sup> However, the large-scale deployment of these renewable energy sources presents several critical challenges, such as energy intermittency, storage limitations, and geographical constraints, which hinder



**Maho Kamiyama**

*Maho Kamiyama is a masters course student at Tohoku University, Japan. She focuses her research on synthesizing diverse nanoclusters and investigating their electrocatalytic activities in Prof. Negishi's group.*



**Tokuhisa Kawawaki**

*Tokuhisa Kawawaki is an Associate Professor in Institute of Multidisciplinary Research for Advanced Materials (IMRAM), Tohoku University, Japan. Previously he served as junior Associate Professor at Tokyo University of Science, Japan. He received his PhD degree in applied chemistry from the University of Tokyo and worked as a Japan Society for the Promotion of Science (JSPS) postdoctoral fellow at the University of Melbourne and a JSPS super postdoctoral fellow at*

*Kyoto University. His current research topics include synthesizing ligand-protected metal nanoparticles and nanoclusters, and their application in photoelectrochemistry as well as photocatalysis.*



**Sourav Biswas**

*Sourav Biswas is an Assistant Professor at IMRAM, Tohoku University, Japan. Before joining here, he served as an Assistant Professor and postdoctoral fellow at Tokyo University of Science, Japan. He obtained his PhD in Chemistry from the National Institute of Technology Durgapur, India and also worked as national post-doctoral fellow at Indian Institute of Science Education and research Thiruvananthapuram, India. His current research interests focus on*

*the synthesis and investigation of potential applications of innovative nanoclusters.*



**Yuichi Negishi**

*Yuichi Negishi is a Professor at IMRAM, Tohoku University, Japan. He received his PhD degree in Chemistry from Keio University. Prior to joining Tohoku University in 2024, he was employed as a Professor at Tokyo University of Science since 2008 and before that worked as an Assistant Professor at Keio University and the Institute for Molecular Science. His research interests include the structural and functional exploration of atomically precise metal NCs, metal NC-*

*assembled materials, and covalent organic frameworks.*

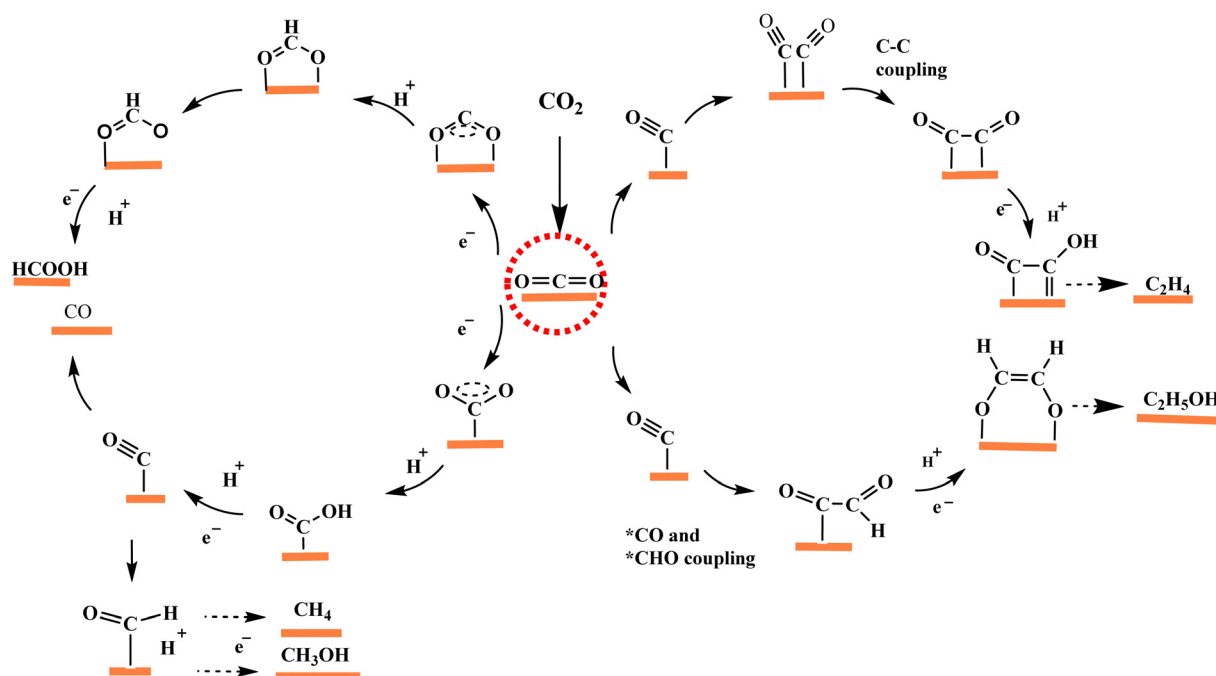
We are honoured to contribute to the celebration of the 10th anniversary of Nanoscale Horizons. Our association with this prestigious journal began in 2021, followed by another publication in 2023—both of which were recognized among the most popular articles of their respective years. We are deeply grateful for the continued opportunity to collaborate with such a prestigious platform. As a gesture of our appreciation and support, we are pleased to contribute once again with this article, in which we explore the potential and future directions of atomically precise metal nanoclusters for electrocatalytic carbon dioxide reduction.



their ability to serve as fully reliable and independent energy solutions.<sup>9,10</sup> As a result, achieving a sustainable energy transition requires the development of diverse alternative energy sources that can overcome existing limitations, ensuring a reliable and efficient energy supply.

In the recent time, capture and conversion of CO<sub>2</sub> into useful fuels have emerged as a game-changer for mitigating both the climate change as well as securing sustainability of energy.<sup>11–14</sup> Among various methodologies, electrochemical CO<sub>2</sub> reduction (ECO<sub>2</sub>R) has garnered significant attention due to its high conversion efficiency, operation under ambient conditions, and ability to generate a wide range of carbon-based fuels such as carbon monoxide (CO), formic acid (HCOOH), methanol (CH<sub>3</sub>OH), methane (CH<sub>4</sub>), ethylene (C<sub>2</sub>H<sub>4</sub>), acetaldehyde (CH<sub>3</sub>CHO), and ethanol (C<sub>2</sub>H<sub>5</sub>OH).<sup>15–19</sup> However, the CO<sub>2</sub> molecule exhibits high thermodynamic and kinetic stability, making its activation and subsequent reduction inherently difficult, which in turn results in sluggish reaction kinetics in ECO<sub>2</sub>R.<sup>20–22</sup> This limitation significantly broadens the scope of catalyst development, as the efficiency and applicability of ECO<sub>2</sub>R are largely dictated by the catalytic material.<sup>23–25</sup> The overall process is governed by the catalyst's ability to regulate reaction selectivity, activity, and stability, making catalyst design a key factor in optimizing the reaction pathway and improving product yield. Industries primarily seek high-energy-value products, such as hydrocarbons, which require multiple proton-coupled electron transfer steps, all orchestrated by the catalyst. Consequently, the design of an ideal electrocatalyst is paramount for unraveling the mechanistic pathway and enhancing product efficiency. The activation of CO<sub>2</sub> is a crucial initial step in the reduction process, and interestingly, CO<sub>2</sub> can adsorb onto the catalyst surface either in a linear or bent configuration. In the case

of linear adsorption, the inherent stability of CO<sub>2</sub> necessitates a significantly high negative potential to induce the formation of the \*CO<sub>2</sub>\*<sup>−</sup> intermediate *via* single-electron capture (Scheme 1). In the subsequent step CO<sub>2</sub> can bind to the catalyst surface either through its two oxygen atoms or *via* the central carbon atom, leading to the formation of distinct intermediates that ultimately dictate the final product selectivity. The HCOO\* intermediate primarily form through proton-coupled electron transfer process when the O atom of \*CO<sub>2</sub>\*<sup>−</sup> is weakly bind with catalyst surface, favoring the formation of HCOOH as the final product. Conversely, if the bond between the carbon of \*CO<sub>2</sub>\*<sup>−</sup> and the catalyst surface is stronger, the \*COOH intermediate is more likely to form.<sup>26</sup> This intermediate further undergoes proton and electron coupling to generate \*CO, a pivotal intermediate in the reaction pathway that influences the formation of both C<sub>1</sub> and C<sub>2</sub> products. \*CO can either desorb from the catalyst surface as CO or undergo further protonation and electron transfer to form C<sub>1</sub> products such as CH<sub>4</sub> and CH<sub>3</sub>OH *via* \*CHO and \*COH intermediates. The formation of C<sub>2</sub> products follows more complex mechanisms due to the distinct energy barriers associated with different intermediates. Significant C<sub>2</sub> intermediates, including \*COCO, \*COCHO, and \*COCOH, arise from the dimerization of \*CO or its interaction with \*CHO and \*COH. Notably, \*COCO is formed through the coupling of two \*CO units, representing an additional rate-determining step in the C<sub>2</sub> product pathway.<sup>27</sup> Furthermore, \*COCHO and \*COCOH can emerge either from the protonation of \*COCO or through direct reactions between \*CO and \*CHO or \*COH. In recent years, researchers have made considerable progress in developing electrocatalysts with moderate selectivity for desired products in ECO<sub>2</sub>R, leveraging different intermediate pathways to enhance efficiency and control over product distribution. For instance, Wang *et al.* reported a CuBr nanoparticle (NP)



Scheme 1 Reaction mechanism of ECO<sub>2</sub>R with different products.



with *in situ* restructuring ability to form Br doped Cu NP during the ECO<sub>2</sub>R process which shows faradaic efficiency (FE) of 91.6% for HCOOH formation at a current density 15.1 mA Cm<sup>-2</sup> under the potential -0.94 V vs. reversible hydrogen electrode (RHE).<sup>28</sup> Jiwanti *et al.* reported a SnO-SnO<sub>2</sub>/Ti<sub>3</sub>C<sub>2</sub>T<sub>x</sub> NP for the ECO<sub>2</sub>R resulting HCOOH of 21.32 ppm with a FE of 94.06% using a boron doped diamond electrode.<sup>29</sup>

Transition metal-based catalysts, particularly in the form of NPs, have garnered significant interest for ECO<sub>2</sub>R due to their inherent stability and high catalytic efficiency.<sup>30–33</sup> These catalysts are crucial in enabling key reaction steps by offering active sites that enhance CO<sub>2</sub> activation and drive its conversion into value-added products. However, despite their promising catalytic properties, several intrinsic challenges limit their overall performance and reproducibility. One of the primary concerns is the inherent heterogeneity in NP size distribution and morphology, which leads to significant variations in catalytic activity and product selectivity.<sup>33</sup> Additionally, the presence of multiple types of active sites within these nanomaterials can introduce complex reaction pathways, often resulting in inconsistent product yields and reduced selectivity for desired products. To overcome these challenges and improve the reliability of nanomaterials for CO<sub>2</sub> reduction, the development of catalysts with uniform particle size and well-defined active sites is crucial. In this context, atomically precise metal nanoclusters (NCs) have recently emerged as a highly promising alternative, offering precise control over size, morphology, and surface composition at the atomic level.<sup>34,35</sup> Unlike conventional NPs, NCs consist of a discrete number of metal atoms, often with well-defined ligand environments, leading to unique electronic structures and distinct catalytic properties. This atomic-level precision enables a more systematic investigation of structure–activity relationships, allowing for the rational design of catalysts with enhanced selectivity, stability, and efficiency for ECO<sub>2</sub>R. In recent years, the ECO<sub>2</sub>R has seen remarkable progress in catalyst design, particularly with atomically precise structural architectures. Numerous studies have been published on this topic, and ongoing research continues to expand our understanding of the fundamental mechanisms and optimization strategies for catalytic performance.<sup>35–38</sup> Although a few review articles summarize the current advancements, they often do not comprehensively cover the most recent breakthroughs, leaving gaps in consolidating the latest developments.<sup>35,39–44</sup> Despite significant progress, a systematic and well-defined approach to identifying the optimal catalyst design—one that ensures both high selectivity and efficiency in product formation—remains lacking. Given the complexity of ECO<sub>2</sub>R, narrowing down the methodologies to determine the most effective strategies is crucial for advancing the field. Therefore, our approach focuses on addressing this gap by critically analyzing existing methodologies and establishing a well-organized framework for designing highly selective and efficient catalysts. Specifically, we aim to leverage atomically precise NCs as model systems to elucidate structure–property relationships and uncover favourable pathways for catalyst development in ECO<sub>2</sub>R.

## 2. Nanoclusters and their effects

Metal NCs consist of a few to a few hundred metal atoms held together predominantly by metallophilic interactions within a sub-3 nm length scale.<sup>45–47</sup> Due to their ultra-small dimensions, quantum confinement effects play a crucial role in defining their electronic structures, setting them apart from their bulk and NP counterparts. Unlike metal NPs, where electronic bands are continuous, NCs exhibit discrete, quantized energy levels, which impart them with unique molecular-like properties.<sup>48–50</sup> In addition, metal NCs exhibit strong structure–property correlation, wherein precise tuning of their electronic charge states necessitates controlled modifications in their structural framework. This fine modulation is predominantly governed by metal–ligand interactions, which dictate both the stability and reactivity of the NCs.<sup>51–58</sup> Consequently, optimizing these interactions is critical for tailoring the physicochemical properties of NCs for specific applications.<sup>59–64</sup>

The molecular-like nature of NCs, with their well-defined geometric and electronic structures, presents new opportunities for enhancing catalytic performance. Through electronic and geometric modifications, their catalytic activity can be systematically tuned to achieve superior efficiency. This advantage is particularly significant in electrocatalysis, where NCs provide a promising platform for designing next-generation catalysts with enhanced activity, selectivity, and stability. In the context of ECO<sub>2</sub>R, NCs are emerging as advanced catalysts due to their precisely defined active sites and tuneable charge states.<sup>34,35,65</sup> Their structural specificity allows for in-depth mechanistic investigations, facilitating the identification of optimal active sites and reaction pathways. This mechanistic understanding is crucial for the rational design of highly efficient catalysts for CO<sub>2</sub> conversion, thereby contributing to the advancement of sustainable energy solutions. As a result, metal NCs are at the forefront of contemporary electrocatalysis research, offering an exciting avenue for the development of innovative catalytic systems with superior performance for ECO<sub>2</sub>R and other important transformations.

### 2.1. Effect of noble metal NCs

The application of NCs in ECO<sub>2</sub>R initially focused on noble metal catalysts, specifically gold (Au) and silver (Ag) NCs, due to their superior stability compared to other transition metal NCs.<sup>34</sup> Among these, Au NCs demonstrated remarkable catalytic performance in CO<sub>2</sub> reduction. In a pioneering study conducted in 2012, Kauffman *et al.* investigated the catalytic efficiency of previously synthesized atomically precise [Au<sub>25</sub>(PET)<sub>18</sub>]<sup>-</sup> (PET: phenylethylthiolate) [Au<sub>25</sub>]<sup>-</sup> NCs (Fig. 1a) in ECO<sub>2</sub>R and compared their performance with Au NPs and bulk Au surfaces.<sup>66,67</sup> Their findings revealed that [Au<sub>25</sub>]<sup>-</sup> NC (1.2 nm) exhibited an exceptionally high FE<sub>CO</sub>, reaching ≈100% at an applied potential of -0.973 V vs. RHE. This efficiency was significantly enhanced compared to other Au-based catalysts: approximately 1.2 times higher than 2 nm Au NPs, 10 times greater than 5 nm Au NPs, and nearly 80 times superior to bulk Au (Fig. 1b). The remarkable catalytic performance of [Au<sub>25</sub>]<sup>-</sup> NC was attributed to





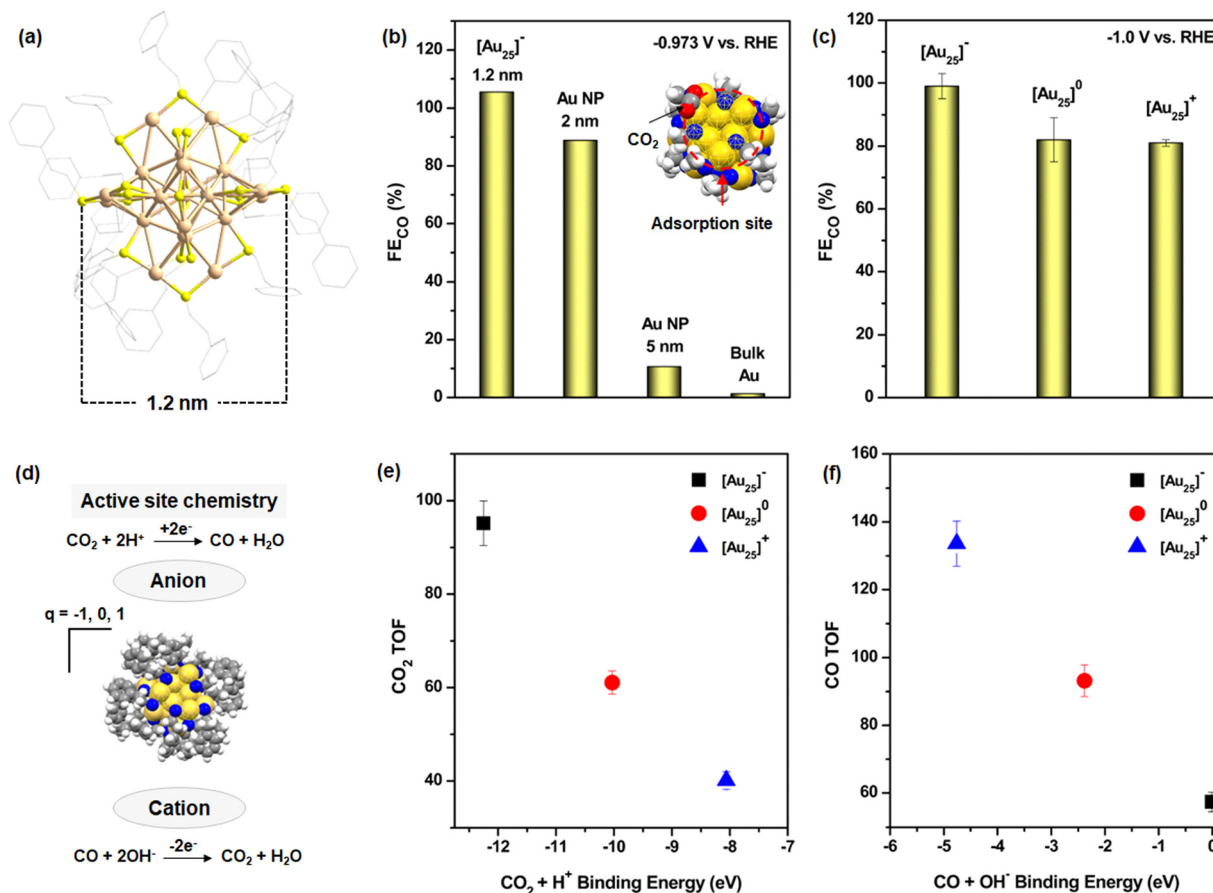


**Fig. 1** (a) Structural architecture of  $[\text{Au}_{25}]^-$  NCs. H atoms are omitted for the clarity. Color legend: Au, tan; S, yellow; and C, gray. (b) Comparison of  $\text{FE}_{\text{CO}}$  among of  $[\text{Au}_{25}]^-$  NC, Au NPs and bulk Au surface. Inset showing the active sites for  $\text{CO}_2$  adsorption in the theoretically model structure. Color legend: Au, gold; S, blue; C, gray; H, white; and O, red. (c) Comparison of  $\text{FE}_{\text{CO}}$  in  $[\text{Au}_{25}]$  NCs depending on their charge. (d) Active site chemistry of  $[\text{Au}_{25}]^-$  NC depending on their charge. (e) and (f) Binding energy vs. reaction TOF for (e)  $\text{CO}_2$  reduction at  $-1 \text{ V vs. RHE}$  and (f) CO oxidation at  $+0.89 \text{ V vs. RHE}$ .

its well-defined molecular structure, which facilitated binding interactions with  $\text{CO}_2$  molecules at the active catalytic site, where O atom of  $\text{CO}_2$  interacts with the three associated S atoms in the shell, partially driven by electrostatic attraction (inset Fig. 1b). These interactions facilitated selective activation of the  $\text{C}=\text{O}$  bond and promoted the formation of surface-adsorbed hydrogen species, which are crucial intermediates in the  $\text{CO}_2$  reduction process. In contrast, such precise catalytic sites and interactions were either absent or significantly less effective in larger Au NPs and bulk Au surfaces, underscoring the advantages of atomically precise NCs in  $\text{ECO}_2\text{R}$ . Although this study achieved the highest  $\text{FE}_{\text{CO}}$  using  $[\text{Au}_{25}]^-$  NCs, it also paved the way for further exploration of other NCs for  $\text{ECO}_2\text{R}$ . This breakthrough also inspired researchers to investigate the influence of structural architecture, electronic charge, and ligand environment on the catalytic performance of NCs. Building on their initial work, the same research group conducted an in-depth study on the role of NC charge in dictating the mechanistic pathway of  $\text{ECO}_2\text{R}$ .<sup>68</sup> They discovered that the charge state of the NC significantly impacted catalytic reactivity by stabilizing the reactant or key reaction intermediates, ultimately influencing the final product yield. Their study concluded that anionic NCs exhibited superior

catalytic performance in terms of  $\text{FE}_{\text{CO}}$  compared to neutral or cationic NCs (Fig. 1c). This enhancement was attributed to the negatively charged NCs, which facilitated  $\text{CO}_2$  adsorption and stabilized key intermediates, thereby improving overall reaction efficiency (Fig. 1d). This was determined through the reaction turnover frequency measured at  $-1 \text{ V vs. RHE}$  in the presence of both acidic and alkaline electrolytes (Fig. 1e and f). Subsequent research efforts led to modifications in the electrochemical setup, transitioning from conventional H-type cells to gas diffusion electrode-based flow electrolyzers which change the mechanistic pathway of the reduction process and the stabilization of the key intermediates, however the final yield is  $\text{CO}$ .<sup>69</sup>

Further investigations delved into the influence of NC size and geometric structure while ensuring that the ligand environment remained consistent. A series of Au NCs from  $\text{Au}_{25}(\text{SC}_6\text{H}_{13})_{18}$ ,  $\text{Au}_{38}(\text{SC}_6\text{H}_{13})_{24}$ , and  $\text{Au}_{144}(\text{SC}_6\text{H}_{13})_{60}$ —previously synthesized, were systematically examined to assess their catalytic performance.<sup>70–73</sup> The results demonstrated that as the Au NC size increased, catalytic activity improved, leading to higher TOF values (Fig. 2a). This suggests a size-dependent influence on reaction kinetics or active site availability. Despite



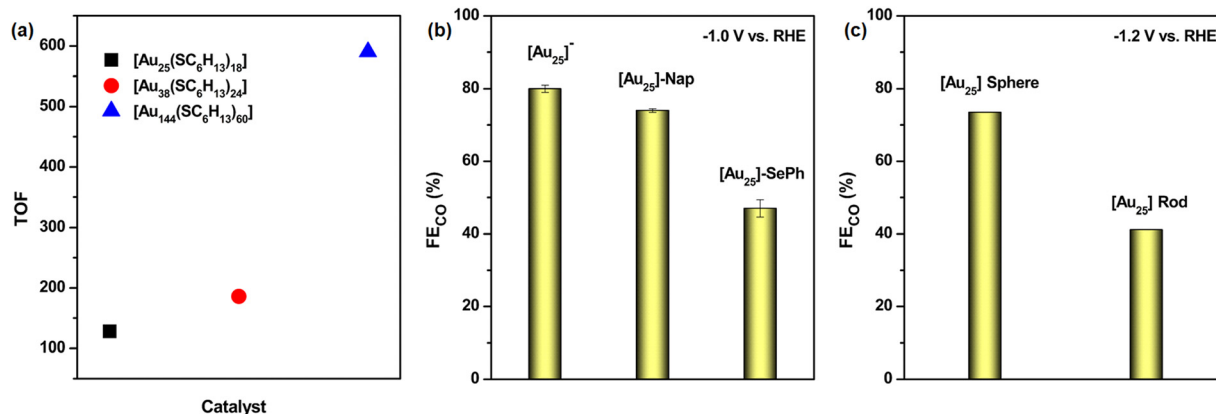


Fig. 2 (a) TOF comparison in  $-0.56$  V vs. RHE among  $\text{Au}_{25}(\text{SC}_6\text{H}_{13})_{18}$ ,  $\text{Au}_{38}(\text{SC}_6\text{H}_{13})_{24}$ , and  $\text{Au}_{144}(\text{SC}_6\text{H}_{13})_{60}$  NCs. (b) Comparison of  $\text{FE}_{\text{CO}}$  among of  $[\text{Au}_{25}]$  NCs with ligand variation. (c) Comparison of  $\text{FE}_{\text{CO}}$  in  $[\text{Au}_{25}]$  NCs depending on their morphology.

these variations in nuclearity and geometric arrangement, all three NCs ultimately facilitated the reduction reaction, yielding CO as the final product, consistent with previous findings. Subsequent research investigated the influence of surface-protecting ligands in  $\text{ECO}_2\text{R}$  while preserving a consistent NC structural framework. This study focused on three  $\text{Au}_{25}$  NCs, each stabilized by distinct ligands: PET, 1-naphthalenethiolate (Nap), and benzoselenolate (SePh).<sup>74</sup> It has been observed that modifications in the carbon tail of the ligands had minimal influence on the reaction outcome, provided that the overall NC framework remained unchanged. However, altering the connecting atoms between the ligand and the NC core had a pronounced effect on product selectivity. For instance, when sulfur (S) was used as the anchoring atom, the reduction reaction predominantly yielded CO as the final product. In contrast, substituting S with selenium (Se) significantly altered the reaction pathway, favoring the competitive hydrogen evolution reaction (HER) (Fig. 2b). Additional studies revealed that modifying surface-protecting ligands could be an effective strategy for fine-tuning the electronic structure of Au NCs, especially by controlling the number of available valence electrons, as illustrated in two separate studies involving  $\text{Au}_{28}$  NCs.<sup>75,76</sup> This electronic modulation, in turn, had a direct impact on both the selectivity and efficiency of the  $\text{ECO}_2\text{R}$ . By varying ligand composition, one could influence the electron density around the NC core, thereby modifying the adsorption strength of  $\text{CO}_2$  intermediates and steering the reaction pathway toward specific products. Additionally, it was discovered that steric effects introduced by bulky ligands imposed spatial constraints on active sites, adversely affecting catalytic performance by hindering substrate accessibility and electron transfer efficiency.<sup>77</sup> These findings underscored the dual role of ligand modifications in both electronic and steric regulation, offering valuable insights for designing high-performance NC-based catalysts. Furthermore, even when the overall Au NC size remained constant, differences in ligand isomerism resulted in variations in  $\text{ECO}_2\text{R}$  efficiency.<sup>78</sup> These variations were primarily attributed to subtle rearrangements in the structural architecture of NC, which altered the stabilization energies of key reaction intermediates. Consequently, these changes influenced the

reaction kinetics and product distribution, demonstrating the critical role of ligand orientation in modulating catalytic performance. Despite these changes in catalytic performance, the final reduction products consistently remained CO and the competitive HER, highlighting the inherent limitations imposed by the Au NC. Liu *et al.* modified the surface microenvironment of the nanocluster by incorporating two 2-thiouracil-5-carboxylic acid ligands into the pocket-like cavity of  $[\text{Au}_{25}(\text{p-MBA})_{18}]^-$  (p-MBA: *para*-mercapto-benzoic acid) NC, significantly enhancing the interaction between nitrogen and  $\text{CO}_2$  molecules and thereby improving the  $\text{FE}_{\text{CO}}$  activity compared to the model NC.<sup>79</sup> Later, structural morphology has been identified as a critical factor in determining the  $\text{ECO}_2\text{R}$  activity of Au NCs. Comparative studies between different structural configurations have revealed significant variations in catalytic performance. For instance, the spherical  $[\text{Au}_{25}(\text{PET})_{18}]^-$  NC exhibited a markedly higher  $\text{FE}_{\text{CO}}$  than the rod-shaped  $[\text{Au}_{25}(\text{PPh}_3)_{10}(\text{PET})_5\text{Cl}_2]^{2+}$  NC (Fig. 2c).<sup>80</sup> This disparity was attributed to the more favourable interaction dynamics between negatively charged reaction intermediates and the active catalytic sites in the spherical NC, facilitating enhanced reaction efficiency. Beyond structural morphology, recent investigations have also emphasized the critical role of hydrides in Au NCs in dictating  $\text{ECO}_2\text{R}$  efficiency.<sup>81</sup> The presence and accessibility of these hydrides significantly influence electron transfer dynamics and intermediate stabilization, thereby affecting the overall reaction pathway. Studies on bridged structures have provided further insights into their catalytic contributions, shedding light on their potential role in optimizing selectivity and efficiency.<sup>82</sup> The presence of alkali metal ions in the electrocatalyst has also been identified as a stimulative factor for  $\text{ECO}_2\text{R}$  when using model  $\text{Au}_{25}$  NC, attributed to the cation-coupled electron transfer step.<sup>83</sup> Despite significant progress in understanding the complex interplay between morphology, ligand effects, and both the geometrical and electronic structures of Au NCs, the  $\text{ECO}_2\text{R}$  using these NCs has largely been limited to CO as the primary reduction product. One of the key challenges hindering further advancement is the persistent competition with HER, which remains a dominant side reaction. This competition effectively limits the efficiency and selectivity of  $\text{CO}_2$  reduction processes. Therefore, there is a critical need for the



development of other materials that can enhance the selectivity for desired products, improve catalytic efficiency, and minimize the impact of side reactions like HER.

Researchers then shifted their focus toward Ag NCs as potential catalysts for ECO<sub>2</sub>R.<sup>40</sup> Compared to their larger Ag NP counterparts, Ag NCs demonstrated significantly enhanced ECO<sub>2</sub>R performance, making them promising candidates for improving reaction efficiency and selectivity. Experimental studies revealed that Ag NCs could achieve nearly 20 times higher CO mass production than Ag NPs, emphasizing their superior catalytic activity in ECO<sub>2</sub>R.<sup>84</sup> However, when comparing with Au NCs containing the same number of metal atoms, such as [Au<sub>25</sub>]<sup>−</sup> and [Ag<sub>25</sub>(SPhMe<sub>2</sub>)<sub>18</sub>]<sup>−</sup> (Ag<sub>25</sub>) (SPhMe<sub>2</sub>: 2,4-dimethyl-benzenethiolate) NCs (Fig. 3a), a significant disparity in CO production efficiency is evident.<sup>85,86</sup> Experimental studies have shown that the Au<sub>25</sub> NC exhibits a much higher FE<sub>CO</sub> and current density than its Ag<sub>25</sub> counterpart, despite both NCs possessing structurally similar active catalytic sites (Fig. 3b). The variation in the onset potential ( $\eta$ ) is also visible. This variation in catalytic performance is primarily attributed to differences in their electronic structures, which influence the required limiting potential for CO<sub>2</sub> reduction. Specifically, the Au<sub>25</sub> NC requires a lower overpotential to activate CO<sub>2</sub> *via* \*COOH intermediate stabilization compared to the Ag<sub>25</sub> NC. The stronger stabilization of the \*COOH intermediate in Au<sub>25</sub> facilitates a more efficient reaction pathway, leading to improved CO<sub>2</sub> conversion rates. In contrast, the Ag<sub>25</sub> NC required a higher overpotential to achieve the same level of activation, which in turn reduced its catalytic efficiency. These findings highlight the superior reactivity of Au NCs over Ag NCs in ECO<sub>2</sub>R, emphasizing the critical role of electronic structure and intermediate stabilization in determining catalytic performance. While Ag NCs offer advantages over conventional Ag NPs, Au NCs remains more efficient catalysts for selective CO<sub>2</sub> reduction, necessitating further optimization of Ag-based NCs to bridge this performance gap. As previously discussed in the case of Au NCs, ligand chemistry plays a pivotal role in modulating both the selectivity and efficiency of the ECO<sub>2</sub>R. A similar influence is observed in Ag NCs, where the nature of the

surface-protecting ligands profoundly affects catalytic performance by altering electronic properties, active site accessibility, and intermediate stabilization. In Au NCs, thiolate ligands have been shown to impact CO selectivity by tuning the electronic structure and binding affinity of key intermediates. However, Ag NCs protected by alkynyl ligands have been reported to exhibit an exceptionally high FE<sub>CO</sub>, consistently reaching approximately 95% at an applied potential of −0.6 V *vs.* RHE.<sup>87</sup> A detailed reaction kinetics analysis further revealed that the formation of \*COOH serves as the rate-determining step in Ag NC-mediated ECO<sub>2</sub>R. The efficiency of CO production is therefore directly linked to the ability of the NC to stabilize this key intermediate. Ligands that enhance the stabilization of \*COOH facilitate more efficient CO<sub>2</sub> reduction, thereby increasing the overall CO production rate. The nature of the ligands is also appeared as a decisive factor in this process, even when the core structure and number of metal atoms in the NCs remain unchanged. A striking contrast is observed between Au NCs and Ag NCs regarding the role of ligands in ECO<sub>2</sub>R performance. In Au NCs, thiolate ligands are known to enhance the FE<sub>CO</sub> by fine-tuning the electronic environment around the active catalytic sites and stabilizing crucial intermediates. However, in Ag NCs, thiolate-protected species do not exhibit similarly high CO<sub>2</sub> reduction efficiency. Instead, Ag NCs demonstrate significantly superior ECO<sub>2</sub>R performance when protected by alkynyl ligands rather than thiolate ligands (Fig. 3c).<sup>88</sup> The underlying reaction mechanism suggests that alkynyl ligands, in particular, play a crucial role in facilitating the formation of key reactive intermediates, thereby influencing catalytic efficacy. These ligands are believed to alter the electronic density around the NC core, modulating the adsorption and stabilization of \*COOH, which is widely recognized as the rate-determining intermediate in CO<sub>2</sub> reduction. By promoting a more favourable energy landscape for \*COOH formation and desorption, alkynyl ligands enhance the overall catalytic efficiency of Ag NCs, leading to improved CO selectivity and higher reaction rates. Recently, Chen *et al.* identified the supportive role of inner-sphere Na<sup>+</sup> ions in alkynyl-protected Ag<sub>15</sub> NC, which enhances FE<sub>CO</sub> activity by promoting

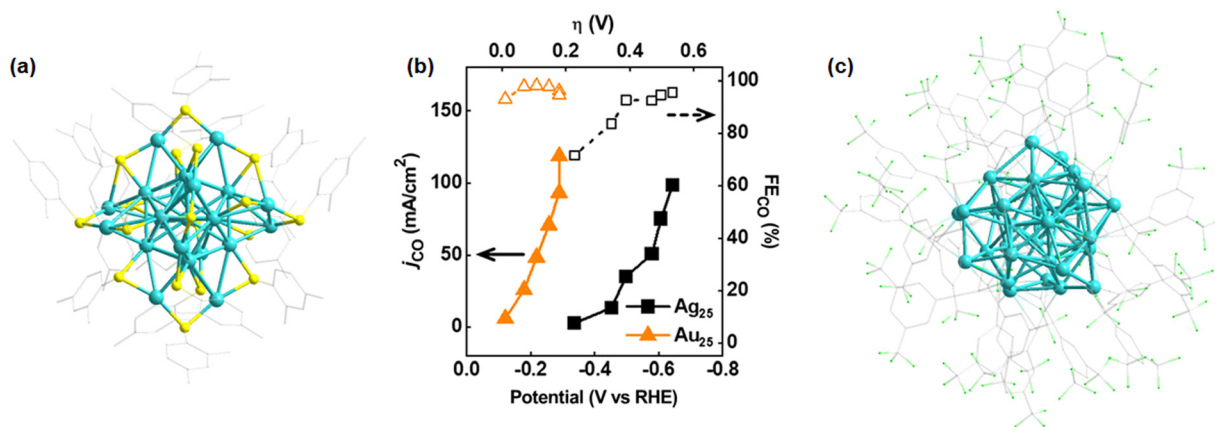


Fig. 3 (a) Structural architecture of Ag<sub>25</sub> NC. H atoms are omitted for the clarity. Color legend: Ag, aqua; S, yellow; and C, gray. (b) Comparison of ECO<sub>2</sub>R data between [Au<sub>25</sub>]<sup>−</sup> and Ag<sub>25</sub> NCs. Reproduced with permission from ref. 85. Copyright 2022 Americal Chemical Society. (c) Structural architecture of alkynyl-protected Ag<sub>32</sub> NC. H atoms are omitted for the clarity. Color legend: Ag, aqua; F, green; and C, gray.



CO<sub>2</sub> activation and facilitating proton transfer through the formation of a Na<sup>+</sup>-CO<sub>2</sub>(\*COOH) complex.<sup>89</sup>

Despite extensive research on Au and Ag NCs for ECO<sub>2</sub>R, a fundamental limitation persists: CO remains the predominant final reduction product, and the reaction is largely confined to a two-electron transfer pathway. While theoretical studies suggest that deeper reductions involving multi-electron transfer processes could lead to value-added products such as hydrocarbons and alcohols, the weak binding stability of key reaction intermediates—such as \*CO, \*CHO, and \*CH<sub>2</sub>—limits further progression along the reduction pathway. As a result, although noble metal NC-based catalysts have demonstrated exceptional efficiency in selectively converting CO<sub>2</sub> to CO, their practical application remains constrained by the inability to achieve more complex reductions. To overcome these limitations and move toward practical implementation, future research must focus on developing alternative catalyst materials capable of stabilizing crucial reaction intermediates. Among the emerging candidates, Cu-based NCs have shown the potential to break the current selectivity bottleneck and unlock new catalytic pathways for CO<sub>2</sub> utilization. Unlike Au and Ag NCs, which primarily facilitate CO evolution, Cu NCs have demonstrated the ability to promote C-C coupling, leading to the formation of multi-carbon products.<sup>90</sup> Despite their promising catalytic activity, Cu NCs face challenges related to stability under electrochemical conditions. However, due to their superior catalytic potential in driving multi-electron CO<sub>2</sub> reduction, Cu NCs are gaining significant attention in the field. Given the rapid development of Cu NCs for ECO<sub>2</sub>R, there is now a pressing need to systematically understand and summarize the various Cu-based NC catalysts that have been utilized for this specific purpose. A comprehensive analysis of their catalytic activity, structural stability, and key influencing parameters—such as ligand effects, electronic properties, and surface morphology—will be essential for understanding their performance trends and optimizing their design. This will not only facilitate the development of next-generation Cu NC catalysts but also contribute to the broader goal of achieving sustainable and selective CO<sub>2</sub> conversion to value-added products.

## 2.2. Effect of Cu NCs

Cu is unique among metal electrocatalysts in its ability to drive ECO<sub>2</sub>R toward a diverse range of C<sub>1</sub> and C<sub>2</sub> products, with over 16 different reduction products identified beyond CO.<sup>91–95</sup> This exceptional versatility stems from Cu's ability to bind CO (\*CO) on its surface with an optimal balance—strong enough to enable further reduction but not so strong as to hinder desorption—while simultaneously stabilizing key reaction intermediates essential for multi-electron transfer processes. In contrast, metals such as Au and Ag exhibit weak CO binding affinities, which favor the evolution of CO as the predominant product rather than its further reduction.<sup>95</sup> On the other hand, metals like nickel (Ni) and platinum (Pt) bind CO too strongly, leading to CO poisoning that deactivates catalytic sites and severely limits their effectiveness in CO<sub>2</sub> reduction. One of the critical factors that set Cu apart is its ability to exist in multiple

oxidation states—Cu<sup>0</sup>, Cu<sup>+</sup>, and Cu<sup>2+</sup>—which dynamically change under reaction conditions and significantly influence product selectivity. Despite these advantages, a major challenge in utilizing Cu NCs for ECO<sub>2</sub>R lies in their low reduction potential, which affects both their stability and the controlled synthesis of well-defined nanostructures. In addition, Cu NCs are highly susceptible to oxidation, aggregation, and surface reconstruction during electrochemical cycling, leading to structural instability and loss of catalytic activity over time. Additionally, their low reduction potential complicates the formation of NCs with precise size and shape control, making it difficult to achieve uniform catalytic behavior. However, significant progress has been made in addressing these limitations through advances in ligand engineering, electrolyte optimization, and surface modification strategies.

The synthesis of ligand-protected stable Cu NCs is typically achieved through the reduction of Cu precursor salts in the presence of surface-protecting ligands, which play a crucial role in stabilizing the resulting NCs.<sup>96,97</sup> However, during the reduction process, Cu enables efficient interaction with a wide range of reaction intermediates that are crucial for converting CO<sub>2</sub> into valuable multi-carbon products.<sup>98</sup> Additionally, Cu nanoclusters (NCs) exhibit a tendency to bind hydride species, which can be introduced through specific reduction methods, potentially influencing the reaction pathway and product selectivity. These hydrides can be accommodated either in interstitial positions within the NC core or as lattice-bound species, both of which significantly alter the overall electronic structure of the NCs. The presence of these hydrides has been shown to have a profound impact on the catalytic efficiency of Cu NCs in ECO<sub>2</sub>R, influencing key reaction intermediates, charge transfer dynamics, and product selectivity. Theoretical studies have provided valuable insights into the role of hydrides in Cu NCs, revealing that these species can modulate the adsorption strength of CO<sub>2</sub>-derived intermediates and directly affect reaction pathways. Given these observations, the subsequent discussion categorizes Cu NCs into two broad groups—hydride-containing Cu NCs and hydride-free Cu NCs—and systematically evaluates their comparative effectiveness in ECO<sub>2</sub>R. Our discussion also aims to provide an in-depth exploration of the intricate mechanisms governing Cu NC-based ECO<sub>2</sub>R, with a particular emphasis on the role of hydride species in modulating reaction selectivity and influencing the structural evolution of the NCs.

**2.2.1. Hydride containing Cu NCs.** The pioneering utilization of Cu NCs in ECO<sub>2</sub>R was demonstrated by Tang *et al.*, who employed the [Cu<sub>32</sub>H<sub>20</sub>(S<sub>2</sub>P(O<sup>i</sup>Pr)<sub>2</sub>)<sub>12</sub>] (S<sub>2</sub>P(O<sup>i</sup>Pr)<sub>2</sub>: diisopropyl dithiophosphate) (Cu<sub>32</sub>) NC, originally synthesized by Dhayal *et al.*<sup>99,100</sup> Cu<sub>32</sub> NC features a distorted hexacapped rhombohedral core composed of fourteen Cu atoms, positioned between two nest-like triangular Cu<sub>9</sub> cupola fragments (Fig. 4a). The structure is further stabilized by twelve dithiophosphate ligands and twenty hydride atoms, which occupy both interstitial and lattice positions. Among these twenty hydrides, twelve are coordinated to the lattice through a tricoordination mode, while six hydrides are attached *via* tetracoordination,





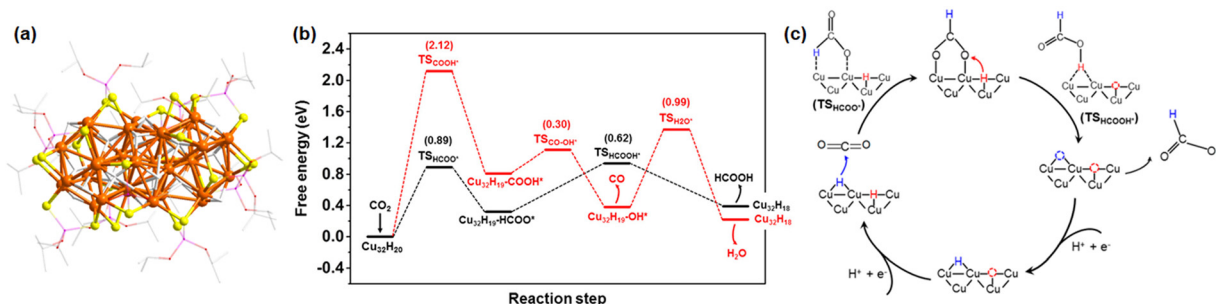


**Fig. 4** (a) Structural architecture of Cu<sub>32</sub> NC. H atoms are omitted partially for the clarity. Color legend: Cu, brown; S, yellow; P, magenta stick; O, red stick; C, gray stick; and H, white. (b) Theoretical Free energy calculations for CO and HCOOH formation by Cu<sub>32</sub> NC. (c) Mechanistic pathway for HCOOH formation from CO<sub>2</sub> reduction. Reproduced with permission from ref. 100. Copyright 2017 Americal Chemical Society.

and the remaining two are pentacoordinated at interstitial positions. Although theoretical Bader charge analysis did not explicitly classify these hydrides based on charge densities, theoretical calculations revealed that the exposed lattice hydride sites serve as favorable binding sites for CO<sub>2</sub>. Notably, among all the lattice-bound hydrides, those located at the periphery of the cupola fragments were identified as the most reactive positions for CO<sub>2</sub> adsorption. Following CO<sub>2</sub> adsorption on the NC surface, the next crucial step in the reduction pathway involves the addition of the first hydrogen atom. To determine whether this proton originates from the lattice hydride positions or the surrounding electrolyte, Tang *et al.* investigated both possible mechanisms (Fig. 4b). Their computational and experimental studies confirmed that the HCOO\* intermediate is preferentially formed *via* the lattice-hydride pathway. Further reduction through the lattice-hydride channel directly leads to the formation of HCOOH as the final product (Fig. 4c). Despite being utilized during the reaction, the lattice hydrides can be regenerated through proton transfer from the electrolyte, ensuring their continued participation in the catalytic cycle. Experimental findings strongly support this mechanism, particularly at low overpotentials, where HCOOH selectivity exceeds 80% with minimal CO and H<sub>2</sub> formation. However, at higher overpotentials, the selectivity shifts as all hydride channels become active, leading to enhanced HER

activity. This study highlights the unique role of lattice hydrides in Cu NCs, suggesting that the lattice-hydride mechanism could serve as a general strategy for achieving selective CO<sub>2</sub> reduction, offering a distinct advantage over conventional electrocatalysts.

To further investigate the role of hydrides in Cu NCs and their impact on ECO<sub>2</sub>R selectivity, Li *et al.* conducted a comprehensive theoretical study.<sup>101</sup> Their work focused on the [Cu<sub>25</sub>H<sub>22</sub>(PPh<sub>3</sub>)<sub>12</sub>]Cl (Cu<sub>25</sub>) NC, which contains a higher number of lattice hydrides compared to previously studied systems. This NC features a well-defined Cu<sub>13</sub> icosahedral core that is further stabilized by four Cu<sub>3</sub> triangular units, which cap the tetrahedral sites of the core. Unlike the previously discussed Cu<sub>32</sub> NC, where hydrides were distributed between both interstitial and lattice positions, in Cu<sub>25</sub> NC, all twenty-two hydrides are exclusively located in lattice positions, each adopting distinct coordination modes. DFT calculations revealed that, similar to earlier findings, the most negatively charged lattice hydrides play a crucial role in facilitating the initial adsorption of CO<sub>2</sub>. The study identified that these lattice hydrides preferentially promote the formation of the HCOO\* intermediate, which subsequently leads to the production of HCOOH. In contrast, the formation of the \*COOH intermediate, a key precursor for CO production, was found to be thermodynamically unfavorable in the presence of lattice hydrides. This computational insight aligns well with previous experimental findings, reinforcing the idea that

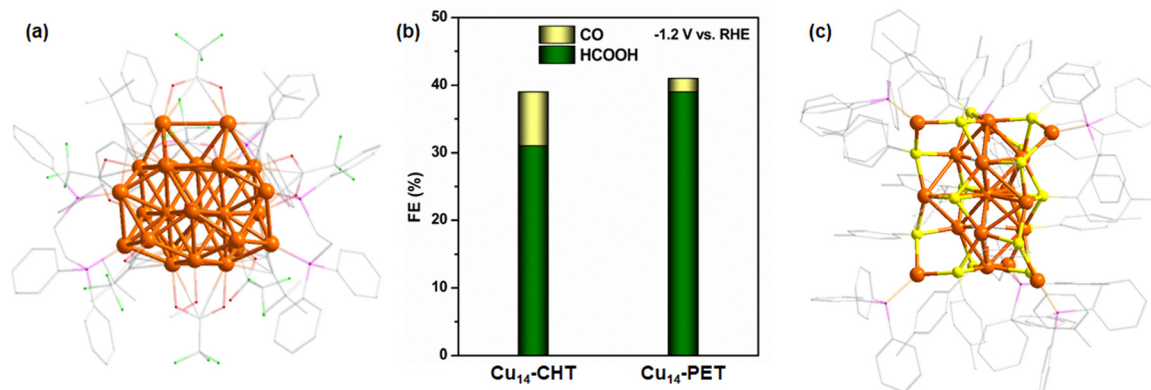


**Fig. 5** (a) Structural architecture of Cu<sub>26</sub> NC. H atoms are omitted for the clarity. Color legend: Cu, brown; P, magenta stick; Cl, green stick; O, red stick; and C, gray stick. (b) Comparison of FE between Cu<sub>14</sub>-CHT and Cu<sub>14</sub>-PET NCs. (c) Structural architecture of Cu<sub>26</sub> NC. H atoms are partially omitted for the clarity. Color legend: Cu, brown; P, magenta stick; C, gray stick; and H, white.



lattice-bound hydrides serve as active catalytic sites that influence product selectivity in  $\text{ECO}_2\text{RR}$ . Li *et al.* synthesized a unique thiol-free  $[\text{Cu}_{26}\text{H}_{11}(\text{DPPE})_3(\text{CF}_3\text{CO}_2)_8(\text{CH}_3\text{O})_2(\text{BuC}\equiv\text{C})_4]^+$  (DPPE: 1,2-bis(diphenylphosphino)ethane) ( $\text{Cu}_{26}$ ) NC which features a distinctive nested structure composed of a tetrahedral  $\text{Cu}_4$  core encapsulated by  $\text{Cu}_6$  and  $\text{Cu}_{16}$  shells (Fig. 5a).<sup>102</sup> The precise positions of the hydride atoms within the NC were determined using theoretical calculations, which confirmed that all eleven hydrides are located in interstitial positions, rather than lattice sites. This structural characteristic significantly influences the catalytic behavior of  $\text{Cu}_{26}$  NC in  $\text{ECO}_2\text{R}$ , as the absence of accessible lattice-bound hydrides limits their direct participation in the reaction. Due to the lack of available lattice hydrides, the adsorption and subsequent reduction of  $\text{CO}_2$  follow an alternative mechanistic pathway in  $\text{Cu}_{26}$  NC, which ultimately leads to the stabilization of the  $^*\text{COOH}$  intermediate rather than the  $\text{HCOO}^*$ . This shift in intermediate formation dictates the final product selectivity, favoring CO evolution over HCOOH. Experimental results demonstrated that  $\text{Cu}_{26}$  NC achieves a FE of 81% for CO production at an applied potential of  $-0.8\text{ V}$  vs. RHE, highlighting its strong selectivity toward  $\text{CO}_2$ -to-CO conversion. To further investigate the role of hydrides in  $\text{ECO}_2\text{R}$ , a comparative theoretical study was performed on the optimized structure of  $\text{Cu}_{26}$ , both with and without hydrides. The results revealed that in the as-synthesized  $\text{Cu}_{26}$  NC, the energy barrier for the formation of the  $^*\text{COOH}$  intermediate was 1.35 eV, whereas the energy barrier for the competing HER was significantly lower at 0.16 eV. This energy difference suggests that in the presence of interstitial hydrides, HER is more favorable than  $\text{CO}_2$  reduction. However, when hydrides were removed from the NC, the energy barrier for  $^*\text{COOH}$  formation drastically decreased from 1.35 eV to 0.14 eV, indicating a substantial enhancement in  $\text{CO}_2$  activation. Additionally, the absence of hydrides shifted the rate-determining step to  $^*\text{CO}$  formation, and the energy barrier for HER increased to 0.72 eV. This increase in HER energy barrier suggests that without hydrides,  $\text{CO}_2$  reduction becomes the dominant process, effectively suppressing hydrogen evolution.

Our research group has also made significant contributions to this field by synthesizing a variety of hydride-containing Cu NCs and evaluating their catalytic performance in  $\text{ECO}_2\text{R}$ . Recently, we conducted a comparative study on two structurally similar yet distinct hydride-containing  $\text{Cu}_{14}$  NCs:  $[\text{Cu}_{14}(\text{PET})_3(\text{PPh}_3)_8\text{H}_{10}]^+$  ( $\text{Cu}_{14}$ -PET) and  $[\text{Cu}_{14}(\text{CHT})_3(\text{PPh}_3)_8\text{H}_{10}]^+$  (CHT: cyclohexanethiolate) ( $\text{Cu}_{14}$ -CHT) NCs.<sup>103</sup> Although these NCs were confirmed to contain hydrides *via* electrospray ionization mass spectrometry (ESI-MS), their precise locations could not be determined through single-crystal X-ray diffraction (SCXRD). However, the experimental findings revealed that  $\text{Cu}_{14}$ -CHT exhibited a maximum FE of 31% for HCOOH and 8% for CO at an applied potential of  $-1.2\text{ V}$  vs. RHE, whereas  $\text{Cu}_{14}$ -PET demonstrated a slightly enhanced FE of 39% for HCOOH and a lower FE of 2% for CO under the same reaction conditions (Fig. 5b). This difference in selectivity highlights the influence of ligand environment and electronic structure on catalytic behavior. Our analysis suggests that the stronger cuprophilic ( $\text{Cu}\cdots\text{Cu}$ ) interactions in  $\text{Cu}_{14}$ -PET lead to a more compact NC structure, which may contribute to

greater stability of key reaction intermediates, ultimately favoring HCOOH formation over CO. Building upon this understanding, we also investigated the catalytic performance of a larger hydride-containing Cu NC,  $[\text{Cu}_{18}\text{H}_2(\text{PTT})_{15}(\text{PPh}_3)_6]$  (PTT: *p*-toluenethiolate) ( $\text{Cu}_{18}$ -PTT) NC (Fig. 5c).<sup>104</sup> The  $\text{ECO}_2\text{RR}$  experiments demonstrated that  $\text{Cu}_{18}$ -PTT achieved a maximum FE of  $\sim 35\%$  for HCOOH and  $\sim 4\%$  for CO at  $-1.2\text{ V}$  vs. RHE. Notably, in this NC, the two hydrides were confirmed to be positioned at interstitial sites rather than lattice positions, meaning they were not directly involved in the proton transfer process during  $\text{CO}_2$  reduction. Despite this,  $\text{Cu}_{18}$ -PTT NC still exhibited a preference for HCOOH production over CO, further reinforcing the hypothesis that factors beyond the presence of lattice hydrides influence catalytic selectivity. A deeper structural analysis of  $\text{Cu}_{18}$ -PTT revealed that its fused-core architecture, featuring a central Cu(0) atom surrounded by strong cuprophilic interactions, played a pivotal role in determining product selectivity. The presence of this metallophilic interaction is believed to modulate the electronic structure of the NC, stabilizing the  $\text{HCOO}^*$  intermediate and promoting HCOOH formation. This finding is particularly significant as it suggests that HCOOH selectivity in Cu NCs is not solely dictated by the presence of lattice hydrides; rather, metallophilic interactions also play a crucial role in tuning catalytic performance. The influence of cuprophilic interactions has also been demonstrated in other studies, where stronger cuprophilic interactions were found to play a crucial role in enhancing catalytic selectivity.<sup>105</sup> Specifically, these interactions have been shown to favor  $\text{CH}_4$  formation by stabilizing key intermediates and facilitating the reaction pathways leading to  $\text{CH}_4$  production.

Later we explored the impact of structural defects on the catalytic performance of Cu NCs, particularly when interstitial hydrides were present.<sup>106</sup> To systematically investigate this, we synthesized and compared three closely related  $\text{Cu}_{58}$  NCs: a regular cubic  $[\text{Cu}_{58}\text{H}_{20}(\text{SPR})_{36}(\text{PPh}_3)_8]^{2+}$  (SPR: propanethiolate) ( $\text{Cu}_{58}$ -I) NC a surface-ligand-vacant distorted  $[\text{Cu}_{58}\text{H}_{20}(\text{SPR})_{36}(\text{PPh}_3)_7]^{2+}$  ( $\text{Cu}_{58}$ -II), and a further distorted variant  $[\text{Cu}_{58}\text{H}_{20}(\text{SET})_{36}(\text{PPh}_3)_6]^{2+}$  (SET: ethanethiolate) ( $\text{Cu}_{58}$ -III) NCs (Fig. 6a–c). These NCs provided an ideal platform to examine how structural distortions, ligand vacancies, and cuprophilic interactions influence  $\text{ECO}_2\text{R}$  product selectivity. In the  $\text{Cu}_{58}$ -I NC, the cubic framework was well-preserved, maintaining a relatively moderate cuprophilic interaction. The interstitial hydrides, though present, were not directly accessible during the catalytic process, which limited its  $\text{CO}_2$  reduction activity. As a result, this NC predominantly facilitated CO evolution, with no significant formation of other products (Fig. 6d). However, when we introduced a surface-ligand vacancy by removing one  $\text{PPh}_3$  ligand from the  $\text{Cu}_{58}$ -I structure, we obtained the  $\text{Cu}_{58}$ -II NC, which featured a partial dislocation of Cu atoms at one of the cube's vertices. This structural modification created an open site that subtly altered the cuprophilic interaction, leading to a distorted geometry. The distortion appeared to stabilize key reaction intermediates, particularly those favoring further proton-coupled electron transfer steps. Consequently,  $\text{Cu}_{58}$ -II NC yielded  $\text{CH}_3\text{OH}$  as the major  $\text{ECO}_2\text{R}$  product, with a FE of  $\sim 44\%$  at  $-0.9\text{ V}$  vs. RHE. This result highlighted the



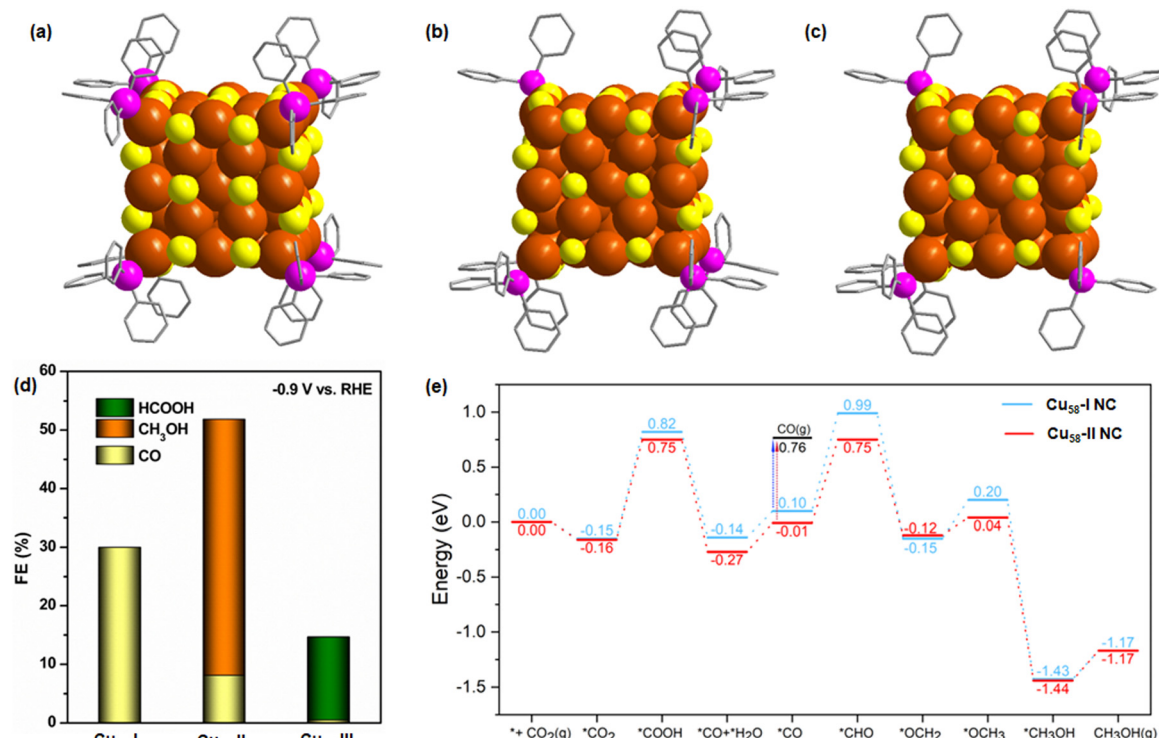


Fig. 6 Structural architecture of (a) Cu<sub>58</sub>-I, (b) Cu<sub>58</sub>-II, (c) Cu<sub>58</sub>-III NCs. H atoms and ligands are partially omitted for the clarity. Color legend: Cu, brown; S, yellow; P, magenta; and C, gray stick. (d) Comparison of FE among Cu<sub>58</sub>-I, Cu<sub>58</sub>-II, Cu<sub>58</sub>-III NCs. (e) Mechanistic insights of the reaction free energy diagram for CO<sub>2</sub> reduction process. Reproduced with permission from ref. 106. Copyright 2025 John Wiley & Sons, Inc.

importance of structural flexibility and ligand vacancy effects in facilitating deeper CO<sub>2</sub> reduction pathways with different stabilization of intermediates (Fig. 6e). Further structural modification in Cu<sub>58</sub>-III NC, achieved by introducing additional Cu atom dislocations at the diagonal vertex of the cube, dramatically influenced the cluster's reactivity. This alteration reoriented the cuprophilic interactions in such a way that it favored competitive HER over CO<sub>2</sub> reduction with very low HCOOH production. This shift suggests that excessive structural distortion and loss of electronic coherence among Cu centers can significantly alter the reaction pathway, ultimately reducing the efficiency of CO<sub>2</sub> reduction and promoting HER. So, these findings provide valuable insights into the delicate balance between NC symmetry, ligand environment, hydride accessibility, and electronic structure in governing ECO<sub>2</sub>R selectivity.

**2.2.2. Hydride free Cu NCs.** Wu *et al.* reported the design and synthesis of a unique [Cu<sub>6</sub>(MBD)<sub>6</sub>] (MBD: 2-mercaptobenzimidazole) (Cu<sub>6</sub>) NC.<sup>107</sup> This hexanuclear NC exhibits a distinct coordination environment in which each Cu(I) atom is simultaneously bonded to both S and nitrogen (N) atoms, a structural feature that arises due to the specific electronic and steric properties of the MBD ligand (Fig. 7a). From our previous discussions, it is evident that this Cu<sub>6</sub> NC does not contain any Cu(0) species, nor does it exhibit any additional metal-metal interactions that could further enhance the typical cuprophilic interaction observed in Cu-based NCs. Moreover, the absence of hydride species suggests that the ECO<sub>2</sub>R likely proceeds *via* the formation of the \*COOH intermediate, which is generated upon

the first protonation of the O site in the adsorbed CO<sub>2</sub> molecule. Consistent with our expectations, the Cu<sub>6</sub> NC achieves a FE of 65.5% for hydrocarbon production at an applied potential of -1.4 V vs. RHE (Fig. 7a). Specifically, it exhibits a product distribution of 42.5% CH<sub>4</sub> and 23% C<sub>2</sub>H<sub>4</sub>, attributed to the effective stabilization of the key \*COOH intermediate. Typically, in Au- and Ag-based NCs, the weak binding affinity of the intermediate readily leads to CO desorption. However, in the case of this Cu<sub>6</sub> NC, such CO release is significantly suppressed due to a favorable binding affinity at the active sites. This enhanced binding affinity arises from the presence of symmetry-broken CuS<sub>2</sub>N<sub>1</sub> coordination sites, which result from the distinct electronegativity and atomic size differences between S and N. This unique coordination environment facilitates stronger adsorption of \*CO, enabling its further hydrogenation to \*CHO and/or participation in C-C coupling reactions. Theoretical energy calculations further support this mechanistic insight, revealing that the energy barrier for CO desorption is relatively high, which promotes \*CHO formation and ultimately dictates the product selectivity toward CH<sub>4</sub> and C<sub>2</sub>H<sub>4</sub>. Moreover, the computed energy profile suggests that the transformation of \*CHO to \*COCHO follows a high-energy pathway (~2.24 eV). This higher activation energy limits the formation of \*COCHO, thereby reducing C<sub>2</sub>H<sub>4</sub> selectivity. Instead, the favored reaction pathway follows \*CHO → \*OCH<sub>3</sub>, leading to an increased yield of CH<sub>4</sub> over C<sub>2</sub>H<sub>4</sub> and consequently resulting in a higher FE for CH<sub>4</sub> production (Fig. 7b). Liu *et al.* systematically investigated the variability in the ECO<sub>2</sub>R efficiency and product selectivity of



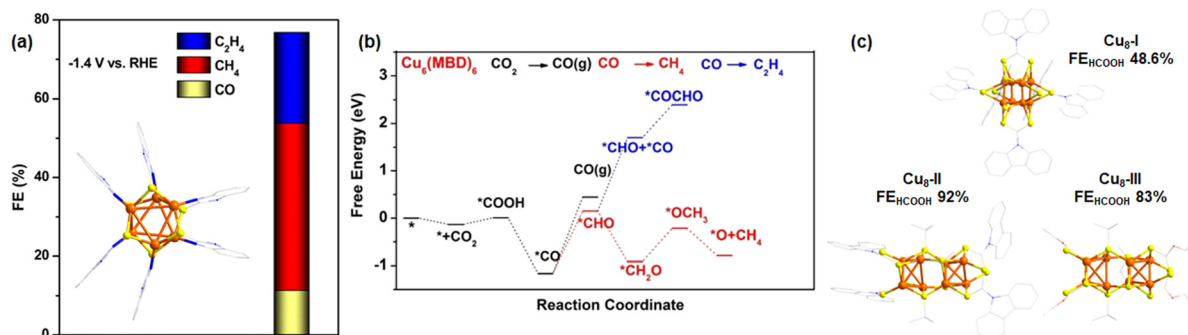


Fig. 7 (a) Structural architecture of [Cu<sub>6</sub>(MBD)<sub>6</sub>] NC and FE. H atoms are omitted for the clarity. Color legend: Cu, brown; S, yellow; N, blue; and C, gray. (b) Theoretical reaction mechanism through free energy profile. Reproduced with permission from ref. 107. Copyright 2023 John Wiley & Sons, Inc. (c) Structural architecture of Cu<sub>8</sub>-I, Cu<sub>8</sub>-II, Cu<sub>8</sub>-III, NCs along with their FE<sub>HCOOH</sub>. H atoms are partially omitted for the clarity. Color legend: Cu, brown; S, yellow; N, blue; O, red.

Cu NCs by altering their structural framework while maintaining a constant Cu atom count per NC unit.<sup>108</sup> Their study revealed that changes in ligand architecture significantly influenced the overall geometric arrangement of Cu NCs, leading to the formation of two distinct Cu<sub>8</sub> NCs: a cube-shaped Cu<sub>8</sub>-I NC and a ditetrahedron-shaped Cu<sub>8</sub>-II NC. Through electrochemical analysis, they identified that the Cu<sub>8</sub>-II NC exhibited almost a double FE for HCOOH (92%) production compared to the Cu<sub>8</sub>-I NC (48.6%) at −1.0 V vs. RHE (Fig. 7c). The difference in ECO<sub>2</sub>R activity between these two NCs was primarily attributed to variations in core arrangements, which induced distinct changes in bond lengths and bond angles, ultimately influencing the stabilization of HCOO\* intermediate, which in turn facilitated the selective production of HCOOH. Additionally, in the same report, Liu *et al.* explored the role of ligands in ECO<sub>2</sub>R by partially modifying the ligand environment of the ditetrahedron-shaped Cu<sub>8</sub>-II NC, resulting in a new variant, Cu<sub>8</sub>-III NC. This ligand alteration induced noticeable changes in FE<sub>HCOOH</sub> ≈ 83%; however, the overall catalytic performance of Cu<sub>8</sub>-III remained superior to that of Cu<sub>8</sub>-I. Thus, this study suggested that modifying the ligand framework not only influenced electronic effects but also affected the stabilization of key intermediates, thereby impacting product selectivity.

Mu *et al.* investigated the role of anion-templated Cu NCs in ECO<sub>2</sub>R. They synthesized two structurally distinct Cu NC variants by employing thiacalix[4]arene and alkynyl ligands as protective frameworks.<sup>109</sup> The first variant was a discrete Cu<sub>38</sub> NC (Fig. 8a), while the second was a hierarchical assembly composed of forty three Cu atoms. From a structural standpoint, their study revealed that the Cu<sub>38</sub> NC exhibited greater intrinsic stability than the Cu<sub>43</sub> NC, which in turn enhanced its applicability for ECO<sub>2</sub>R. Electrochemical studies demonstrated that the Cu<sub>38</sub> NC achieved a maximum FE of 62.01% for hydrocarbon production at an applied potential of −1.57 V vs. RHE (Fig. 8a). The hydrocarbon product distribution consisted of 34.03% C<sub>2</sub>H<sub>4</sub> and 27.98% CH<sub>4</sub>. The theoretical study revealed that the energy barrier for the \*CO → \*COH transition was significantly higher compared to the \*CO → \*OCCO step (Fig. 8b). This energy difference favored the formation of the \*OCCO intermediate, which subsequently facilitated C–C coupling and C<sub>2</sub>H<sub>4</sub> production. Guan *et al.* reported the synthesis and catalytic performance of hydrophobically stabilized Cu<sub>4</sub> NCs supported on multi-walled carbon nanotubes (MWCNTs) for ECO<sub>2</sub>R.<sup>110</sup> They systematically compared the catalytic behavior of these Cu<sub>4</sub> NCs with molecular Cu species embedded in MWCNTs to evaluate their efficiency and product selectivity.

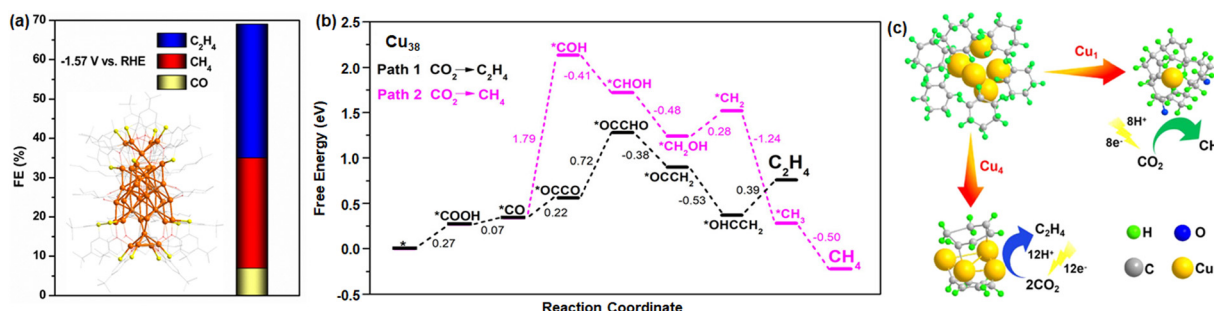


Fig. 8 (a) Structural architecture of Cu<sub>38</sub> NC and FE. H atoms are omitted for the clarity. Color legend: Cu, brown; S, yellow; O, red; and C, gray. (b) Theoretical reaction mechanism through free energy profile. Reproduced with permission from ref. 109. Copyright 2024 Americal Chemical Society. (c) Comparison in ECO<sub>2</sub>R product when Cu NCs embedded on MWCNT. Reproduced with permission from ref. 110. Copyright 2021 Americal Chemical Society.





Their study revealed that the chemically anchored Cu<sub>4</sub> NCs formed stable catalytic sites on the MWCNT surface through strong interactions, which contributed to significantly enhanced selectivity for hydrocarbon products. Notably, they observed a crucial shift in product distribution when the Cu active site changed from a single Cu atom to a tetra-nuclear Cu<sub>4</sub> NC (Fig. 8c). While single Cu atoms predominantly favored CH<sub>4</sub> production, the transition to Cu<sub>4</sub> NCs altered the reaction pathway, leading to a preference for C<sub>2</sub>H<sub>4</sub> formation. This shift in selectivity was attributed to the increased catalytic surface area of the Cu<sub>4</sub> NCs, which promoted the aggregation of active sites. The enhanced surface area facilitated \*CO dimerization, a key intermediate step in C–C bond formation, thereby favoring C<sub>2</sub>H<sub>4</sub> production over CH<sub>4</sub>. Theoretical studies establish that Cu(100) favors C–C coupling and ethylene formation, while Cu(111) preferentially yields methane due to facet-dependent adsorption energies of key intermediates.<sup>111</sup> This effect is more pronounced in NPs and extensively studied in the literature.<sup>112–114</sup> Thus, these findings highlight the critical role of nuclearity in modulating catalytic performance and selectivity in ECO<sub>2</sub>R reactions for Cu NCs.

### 2.3. Effect of alloy NCs

It is evident from the previous discussion that Cu NCs exhibit superior catalytic activity and product selectivity beyond CO compared to overcrowded noble metal NCs. However, further catalyst engineering is necessary to fine-tune the CO<sub>2</sub> reduction pathway, which can be achieved by doping foreign metal atoms into the NCs. Bimetallic or trimetallic catalysts often exhibit superior performance compared to their monometallic counterparts, owing to synergistic effects arising from the interaction between distinct active catalytic centers.<sup>115–117</sup> A pioneering study by Li *et al.* compared the electrocatalytic activity of Pd<sub>1</sub>Au<sub>24</sub> NCs with the well-established Au<sub>25</sub> NC model system.<sup>118</sup> Their results revealed that Pd doping significantly suppressed the competing HER at high currents while maintaining a remarkable 100% FE for CO production over a broad potential range (−0.6 V to −1.2 V vs. RHE). In contrast, Au<sub>25</sub> NCs exhibited a decline in CO selectivity beyond −0.9 V vs. RHE. Theoretical calculations revealed that doping with Pd

significantly increases the thermodynamic barrier for the desorption of thiolate ligands from the nanocluster surface. This enhancement in ligand binding strength leads to greater structural stability of the nanocluster, particularly by preserving the coordination environment around the Au active sites. As a result, the Pd-doped system exhibits improved resilience under electrochemical conditions, which in turn enhances its selectivity for ECO<sub>2</sub>R, especially at higher potentials. Subsequent studies explored the effects of Cd doping in Au NCs, revealing that modifications in surface geometry and electronic structure through narrowing the energy gap altered intermediate binding energies, leading to enhanced CO selectivity in high-potential regions.<sup>119–121</sup> However, despite these advances, both homometallic and bimetallic noble metal NCs predominantly yield CO as the main product, limiting their practical applicability. In contrast, Cu-based catalysts have a unique ability to generate a wider range of products in ECO<sub>2</sub>R, making them more versatile for real-world applications. Given this distinction, the following section will explore the effectiveness of Cu-based doped NCs in ECO<sub>2</sub>R and their potential for optimizing product selectivity. Ma *et al.* reported a series of alkynyl-protected M<sub>15</sub> alloy NCs—Au<sub>7</sub>Ag<sub>8</sub>, Ag<sub>9</sub>Cu<sub>6</sub>, and Au<sub>2</sub>Ag<sub>8</sub>Cu<sub>5</sub>—synthesized using a site-specific metal exchange approach to investigate the role of different metal atoms in the ECO<sub>2</sub>R.<sup>122</sup> Structural analysis revealed that all three NCs adopt a similar core-shell-shell configuration with a well-defined M<sub>core</sub>@M<sub>cube</sub>@M<sub>octahedron</sub> geometry. However, while the central core position remains fixed with Au, variations in the shell composition due to the presence of different metal atoms lead to distinct electronic effects, altering ligand coordination and modifying the active surface motifs. This structural diversification significantly influences catalytic performance in ECO<sub>2</sub>R. The Au<sub>7</sub>Ag<sub>8</sub> NC demonstrated exceptional CO selectivity, achieving a maximum FE of 98.1% at −0.49 V vs. RHE (Fig. 9a). In contrast, Ag<sub>9</sub>Cu<sub>6</sub> and Au<sub>2</sub>Ag<sub>8</sub>Cu<sub>5</sub> NCs predominantly facilitated the production of HCOOH at more negative potentials. These findings highlight the crucial role of Cu in favoring HCOOH formation over CO production. Notably, Ag<sub>9</sub>Cu<sub>6</sub> exhibited a higher FE for HCOOH compared to the trimetallic Au<sub>2</sub>Ag<sub>8</sub>Cu<sub>5</sub> NC, which was attributed to the enhanced stabilization of the HCOO\* intermediate at the Ag–Cu active sites. Deng *et al.* reported the effect of Cu doping in

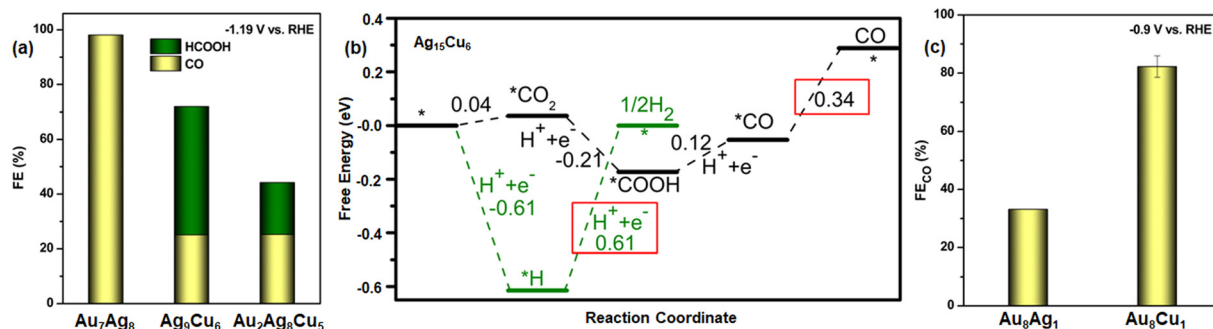


Fig. 9 (a) Comparison of FE series of among alkynyl-protected M<sub>15</sub> alloy NCs. (b) Theoretical reaction mechanism through free energy profile by using Ag<sub>15</sub>Cu<sub>6</sub> NC as catalyst. Reproduced with permission from ref. 123. Copyright 2023 Americal Chemical Society. (c) Comparison of FE with different M<sub>9</sub> alloy NCs.



Ag NCs by synthesizing a core-shell alkynyl-protected  $[\text{Ag}_{15}\text{Cu}_6(\text{C}\equiv\text{CR})_{18}(\text{DPPE})_2]^-$  ( $\text{HC}\equiv\text{CR}$ : 3,5-bis(trifluoromethyl)phenylacetylene) ( $\text{Ag}_{15}\text{Cu}_6$ ) NC.<sup>123</sup> This NC features a body-centered cubic (bcc)  $\text{Ag}_{11}\text{Cu}_4$  core, which follows the  $\text{M}_{\text{core}}@\text{M}_{\text{cube}}@\text{M}_{\text{octahedron}}$  structural motif, with an atomic arrangement of  $\text{Ag}@_{\text{Ag}_8}@\text{Ag}_2\text{Cu}_4$ . The core is further stabilized by two Cu atoms, two  $\text{Ag}_2\text{DPPE}$  motifs, and eighteen alkynyl ligands, contributing to its well-defined structural integrity.  $\text{ECO}_2\text{R}$  studies revealed that  $\text{Ag}_{15}\text{Cu}_6$  NC exhibited superior catalytic efficiency and selectivity, achieving a high  $\text{FE}_{\text{CO}}$  production ( $\text{FE}_{\text{CO}} \sim 91.3\%$  at  $-0.81$  V vs. RHE). This performance was significantly better compared to a structurally similar bcc-type  $\text{Ag}_9\text{Cu}_6$  NC, which displayed a much lower  $\text{FE}_{\text{CO}}$  of 48.5% under similar conditions. They identified that ligand removal from  $\text{Ag}_9\text{Cu}_6$  NC led to a deterioration in catalytic performance, whereas the  $\text{Ag}_{15}\text{Cu}_6$  NC maintained its ligand environment more effectively, preserving its reactivity and selectivity. The free energy profile diagram signifies the stability of the intermediate on the surface of the  $\text{Ag}_{15}\text{Cu}_6$  NC which leads to the formation of CO (Fig. 9b). Further, they extended their synthetic strategy to incorporate Cu doping into Au NCs and successfully synthesized  $[\text{Au}_{15}\text{Cu}_4(\text{DPPM})_6\text{Cl}_4(\text{C}\equiv\text{CR})_4]^{2+}$  (DPPM: bis(diphenylphosphino)methane) NC which exhibited a significantly higher  $\text{FE}_{\text{CO}}$  compared to its undoped counterpart,  $\text{Au}_{18}$  NC.<sup>124</sup> Theoretical calculations revealed that Cu doping induces strong synergistic effects within the NC framework, fundamentally altering the electronic structure and catalytic behavior. In particular, the study suggested that the presence of exposed Au–Cu dual sites played a crucial role in initiating the  $\text{ECO}_2\text{R}$  process. These active dual sites facilitated electron transfer, optimizing the adsorption and activation of  $\text{CO}_2$  molecules. Additionally, Cu incorporation led to a synergistic d-state shift between Au and Cu, which fine-tuned the binding strength of key reaction intermediates, thereby enhancing catalytic efficiency and selectivity. Su *et al.* conducted a comparative study using a model  $\text{M}_9$  NC system, in which partially thiol-capped Au NCs were doped with Cu and Ag to evaluate their effectiveness in  $\text{ECO}_2\text{R}$  effectivity.<sup>125</sup> Electrochemical studies demonstrated that Cu doping significantly enhanced the catalytic activity, with  $[\text{Au}_8\text{Cu}_1(\text{SAdm})_4(\text{Dppm})_3\text{Cl}]^{2+}$  (SAdm: adamantanethiolate) NC achieving a higher  $\text{FE}_{\text{CO}}$  ( $\sim 82.2\%$ ) whereas its Ag-doped counterparts  $[\text{Au}_8\text{Ag}_1(\text{SAdm})_4(\text{Dppm})_3\text{Cl}]^{2+}$  NC exhibited much lower  $\text{FE}_{\text{CO}}$  ( $\sim 33.1\%$ ) (Fig. 9c). Theoretical calculations were performed, revealing that the Au–Cu active surface effectively lowers the energy barrier for  $\text{CO}_2$  reduction and provides enhanced stability to key reaction intermediates. Shi *et al.* recently conducted a theoretical investigation into the catalytic performance of Cu NCs, focusing on the role of surrounding atoms in modulating electrocatalytic activity.<sup>126</sup> They selected  $\text{Cu}_{13}$  and  $\text{Cu}_{55}$  as model NCs, considering their magic-number-associated symmetrical stability, which provides well-defined electronic and geometric structures. To explore the influence of transition metal doping, they systematically substituted the corner atoms of these NCs with widely available transition metals—Fe, Co, and Ni—leading to the formation of a crown jewel structure. Their theoretical findings revealed that multi-atom alloy NCs exhibit significantly enhanced catalytic activity by suppressing

the energy barrier compared to conventional Cu (211) surfaces, which are often considered active sites for  $\text{CO}_2$  reduction on bulk Cu catalysts. Among the different dopants studied, Co incorporation in Cu-based clusters demonstrated the lowest free energy barrier (0.33 eV) for  $\text{CO}_2$  reduction, indicating a highly favorable reaction pathway. Furthermore, their analysis indicated that catalytic performance is largely governed by the relative proportion of metallic dopants, which influences local coordination environments. In particular, a coordination number of six—formed by specific dopant arrangements—was found to be a key structural feature enabling the efficient reduction of  $\text{CO}_2$  to  $\text{CH}_4$ . This study underscores the potential of precise atomic doping strategies in optimizing Cu-based NCs for  $\text{ECO}_2\text{R}$ , offering fundamental insights into the design of highly efficient and selective electrocatalysts.

### 3. Conclusions and outlook

This article provides a comprehensive analysis of recent advancements in atomically precise metal NC-based catalysts for  $\text{ECO}_2\text{R}$ . While noble metal NCs have demonstrated the highest FE for  $\text{CO}_2$  reduction, their catalytic performance is largely limited to the formation of CO, with little diversification in product selectivity. This constraint arises from the intrinsic properties of noble metals, which do not effectively stabilize intermediates required for the formation of more complex reduction products. To overcome this limitation, researchers have explored various factors that influence catalytic activity, including ligand effects, electronic structures, and the introduction of external stimuli. However, despite these efforts, the primary product of  $\text{CO}_2$  reduction using noble metal NCs remains CO, highlighting the need for alternative strategies to expand product selectivity. In contrast, Cu NCs and Cu-based alloy NCs have emerged as promising candidates for broadening the scope of  $\text{ECO}_2\text{R}$  products. Due to their unique electronic structures and intermediate stabilization capabilities, Cu NCs facilitate multi-step reduction processes, leading to the formation of high-value products such as HCOOH, hydrocarbons, and oxygenates. However, the synthesis of Cu NCs poses significant challenges due to their inherent instability. Unlike noble metal NCs, Cu NCs tend to undergo structural degradation, limiting their practical applicability. One promising approach to address this issue involves the incorporation of hydrides, which not only enhance the stability of Cu NCs but also influence product selectivity, particularly favoring the formation of HCOOH. Furthermore, the absence or limited availability of hydrides in the catalytic system has been found to promote deeper reduction pathways, yielding more complex and energy-dense products. In addition to hydride incorporation, various external and internal factors—such as ligand effects, support interactions, and electrochemical conditions—have been studied to optimize Cu NC-based catalysts. The incorporation of Cu into alloy NCs has also proven beneficial, extending the product selectivity window while maintaining high FE. Thus, this review article systematically outlines the stepwise evolution of NC-based catalyst design, detailing the interplay between structural modifications and catalytic performance. By



elucidating the structure–property correlations of NC catalysts, this work provides valuable insights into the rational design of efficient catalysts tailored for selective CO<sub>2</sub> reduction.

Looking ahead, several key challenges and opportunities remain in the development of NC-based catalysts for ECO<sub>2</sub>R. Although Cu-based NCs exhibit considerable catalytic potential influenced by their size, the limited availability of stable high-nuclear Cu NCs continues to hinder the comprehensive exploration of their catalytic properties. This limitation primarily stems from challenges related to their stability. Future research should therefore focus on developing innovative synthetic strategies to obtain high-nuclear Cu NCs with precisely controlled compositions—including both hydride-rich and hydride-free variants—as the presence of hydrides has also been shown to play a crucial role in influencing catalytic activity. Additionally, while Cu is currently the most promising transition metal for selective CO<sub>2</sub> reduction, exploring other transition metal NCs may uncover alternative catalytic pathways, potentially altering intermediate binding affinities and enabling new reaction mechanisms. Furthermore, the scope of alloy-based NC catalysts remains underexplored, particularly in the context of Cu alloying strategies. The integration of additional transition metals into Cu NCs may lead to synergistic effects that enhance stability, selectivity, and catalytic efficiency. Future research should prioritize the rational design of alloy NCs with tunable electronic structures to achieve optimal CO<sub>2</sub> reduction performance. In addition to catalyst design, the configuration of the electrolyzer plays a crucial role in determining the overall efficiency, selectivity, and stability of ECO<sub>2</sub>R. Factors such as electrode architecture, ion transport pathways, and electrolyte composition can significantly influence the reaction environment and, consequently, the catalytic performance. Despite its importance, this aspect remains relatively underexplored, particularly in the context of employing NCs as catalysts. Most studies to date have focused primarily on material development, with limited attention given to optimizing the integration of NCs within practical electrolyzer setups. This presents a valuable opportunity for future research to bridge the gap by systematically investigating the interplay between nanocluster-based catalysts and electrolyzer design, potentially unlocking new avenues for enhancing ECO<sub>2</sub>R efficiency at scale. Ultimately, advancing the field of NC-based electrocatalysis holds immense promise for sustainable and environmentally friendly CO<sub>2</sub> conversion technologies. As research progresses, the continued development of atomically precise NC catalysts will pave the way for transformative breakthroughs in catalytic science, offering new opportunities for industrial and environmental applications. By addressing current challenges and leveraging innovative synthesis strategies, we are poised to unlock the full potential of metal NCs for next-generation CO<sub>2</sub> reduction processes.

## Data availability

No primary research results, software or code have been included and no new data were generated or analysed as part of this review.

## Conflicts of interest

There are no conflicts to declare.

## Acknowledgements

This work was supported by the JSPS KAKENHI (grant no. 23H00289 and 22K19012), Scientific Research on Innovative Areas “Aquatic Functional Materials” (grant no. 22H04562), the Yazaki Memorial Foundation for Science and Technology, Advanced Technology Institute Research Grants, Takahashi Industrial and Economic Research Foundation, and the Kumagai Foundation for Science and Technology and the Ogasawara Foundation for the Promotion of Science and Engineering.

## Notes and references

- 1 S. J. Davis, K. Caldeira and H. D. Matthews, *Science*, 2010, **329**, 1330–1333.
- 2 J. Hansen, M. Sato, R. Ruedy, A. Lacis and V. Oinas, *Proc. Natl. Acad. Sci. U. S. A.*, 2000, **97**, 9875–9880.
- 3 M. Meinshausen, N. Meinshausen, W. Hare, S. C. Raper, K. Frieler, R. Knutti, D. J. Frame and M. R. Allen, *Nature*, 2009, **458**, 1158–1162.
- 4 G. A. Olah, G. S. Prakash and A. Goepfert, *J. Am. Chem. Soc.*, 2011, **133**, 12881–12898.
- 5 K. B. Keerthana, S.-W. Wu, M.-E. Wu and T. Kokulnathan, *Sustainability*, 2023, **15**, 7932.
- 6 S. C. Obiora, O. Bamisile, Y. Hu, D. U. Ozsahin and H. Adun, *Heliyon*, 2024, **10**, e28770.
- 7 P. A. Østergaard, N. Duic, Y. Noorollahi and S. Kalogirou, *Renewable Energy*, 2022, **199**, 1145–1152.
- 8 I. E. Agency, *World energy outlook*, OECD/IEA Paris, 2009.
- 9 D. Gielen, F. Boshell, D. Saygin, M. D. Bazilian, N. Wagner and R. Gorini, *Energy Strategy Rev.*, 2019, **24**, 38–50.
- 10 W. Strielkowski, L. Civi, E. Tarkhanova, M. Tvaronavičienė and Y. Petrenko, *Energies*, 2021, **14**, 8240.
- 11 S. M. Kim, P. M. Abdala, M. Broda, D. Hosseini, C. Copéret and C. Müller, *ACS Catal.*, 2018, **8**, 2815–2823.
- 12 K. M. K. Yu, I. Curcic, J. Gabriel and S. C. E. Tsang, *ChemSusChem*, 2008, **1**, 893–899.
- 13 W. D. Jones, *J. Am. Chem. Soc.*, 2020, **142**, 4955–4957.
- 14 T. P. Senftle and E. A. Carter, *Acc. Chem. Res.*, 2017, **50**, 472–475.
- 15 G. A. Ozin, *Adv. Mater.*, 2015, **27**, 1957–1963.
- 16 D.-H. Nam, P. De Luna, A. Rosas-Hernández, A. Thevenon, F. Li, T. Agapie, J. C. Peters, O. Shekhah, M. Eddaoudi and E. H. Sargent, *Nat. Mater.*, 2020, **19**, 266–276.
- 17 J. Wu, Y. Huang, W. Ye and Y. Li, *Adv. Sci.*, 2017, **4**, 1700194.
- 18 W. Zhang, Y. Hu, L. Ma, G. Zhu, Y. Wang, X. Xue, R. Chen, S. Yang and Z. Jin, *Adv. Sci.*, 2018, **5**, 1700275.
- 19 S. Nitopi, E. Bertheussen, S. B. Scott, X. Liu, A. K. Engstfeld, S. Horch, B. Seger, I. E. L. Stephens, K. Chan, C. Hahn, J. K. Nørskov, T. F. Jaramillo and I. Chorkendorff, *Chem. Rev.*, 2019, **119**, 7610–7672.
- 20 F. Dattila, R. R. Seemakurthi, Y. Zhou and N. López, *Chem. Rev.*, 2022, **122**, 11085–11130.



- 21 X. She, Y. Wang, H. Xu, S. Chi Edman Tsang and S. Ping Lau, *Angew. Chem., Int. Ed.*, 2022, **61**, e202211396.
- 22 J. Han, X. Bai, X. Xu, A. Husile, S. Zhang, L. Qi and J. Guan, *Chem. Sci.*, 2024, **15**, 7870–7907.
- 23 S. Garg, M. Li, A. Z. Weber, L. Ge, L. Li, V. Rudolph, G. Wang and T. E. Rufford, *J. Mater. Chem. A*, 2020, **8**, 1511–1544.
- 24 S. Zhang, Q. Fan, R. Xia and T. J. Meyer, *Acc. Chem. Res.*, 2020, **53**, 255–264.
- 25 C. S. Diercks, Y. Liu, K. E. Cordova and O. M. Yaghi, *Nat. Mater.*, 2018, **17**, 301–307.
- 26 J. Yu, J. Wang, Y. Ma, J. Zhou, Y. Wang, P. Lu, J. Yin, R. Ye, Z. Zhu and Z. Fan, *Adv. Funct. Mater.*, 2021, **31**, 2102151.
- 27 W. Zhang, Y. Yang, D. Guo and L. Liu, *J. Energy Chem.*, 2024, **88**, 10–27.
- 28 X. Wang, A. Guo, Y. Wang, Z. Chen, Y. Guo, H. Xie, W. Shan and J. Zhang, *J. Colloid Interface Sci.*, 2024, **653**, 238–245.
- 29 P. K. Jiwanti, M. A. Jazuli, D. K. A. Sukardi, G. T. M. Kadja, M. Tomisaki, A. Purwaningsih and Y. Einaga, *J. Solid State Electrochem.*, 2025, **29**, 401–411.
- 30 F. Franco, C. Rettenmaier, H. S. Jeon and B. R. Cuenya, *Chem. Soc. Rev.*, 2020, **49**, 6884–6946.
- 31 M. Li, S. Garg, X. Chang, L. Ge, L. Li, M. Konarova, T. E. Rufford, V. Rudolph and G. Wang, *Small Methods*, 2020, **4**, 2000033.
- 32 D. Johnson, Z. Qiao and A. Djire, *ACS Appl. Energy Mater.*, 2021, **4**, 8661–8684.
- 33 T. Zheng, K. Jiang and H. Wang, *Adv. Mater.*, 2018, **30**, 1802066.
- 34 S. Biswas, Y. Shingyouchi, M. Ogami, M. Kamiyama, T. Kawawaki and Y. Negishi, *EcoEnergy*, 2024, **2**, 400–418.
- 35 D. Yang, J. Wang, Q. Wang, Z. Yuan, Y. Dai, C. Zhou, X. Wan, Q. Zhang and Y. Yang, *ACS Nano*, 2022, **16**, 15681–15704.
- 36 K. Kwak and D. Lee, *Acc. Chem. Res.*, 2019, **52**, 12–22.
- 37 J. Huang, N. Hörmann, E. Oveisi, A. Loiudice, G. L. De Gregorio, O. Andreussi, N. Marzari and R. Buonsanti, *Nat. Commun.*, 2018, **9**, 3117.
- 38 T. Liu and H. Yabu, *EcoEnergy*, 2024, **2**, 419–432.
- 39 Y. Liu, J. Yu, Y. Lun, Y. Wang, Y. Wang and S. Song, *Adv. Funct. Mater.*, 2023, **33**, 2304184.
- 40 G. Ma, L. Qin, Y. Liu, H. Fan, L. Qiao, C. Yu and Z. Tang, *Surf. Interfaces*, 2023, **36**, 102555.
- 41 S. Zhao, R. Jin and R. Jin, *ACS Energy Lett.*, 2018, **3**, 452–462.
- 42 T. Kawawaki, T. Okada, D. Hirayama and Y. Negishi, *Green Chem.*, 2024, **26**, 122–163.
- 43 M. Wu, F. Dong, Y. Yang, X. Cui, X. Liu, Y. Zhu, D. Li, S. Omanovic, S. Sun and G. Zhang, *Electrochem. Energy Rev.*, 2024, **7**, 10.
- 44 L. Chen, L. Wang, Q. Shen, Y. Liu and Z. Tang, *Mater. Chem. Front.*, 2023, **7**, 1482–1495.
- 45 R. Jin, C. Zeng, M. Zhou and Y. Chen, *Chem. Rev.*, 2016, **116**, 10346–10413.
- 46 S. Biswas, S. Das and Y. Negishi, *Coord. Chem. Rev.*, 2023, **492**, 215255.
- 47 I. Chakraborty and T. Pradeep, *Chem. Rev.*, 2017, **117**, 8208–8271.
- 48 Y. Du, H. Sheng, D. Astruc and M. Zhu, *Chem. Rev.*, 2020, **120**, 526–622.
- 49 X. Kang and M. Zhu, *Chem. Soc. Rev.*, 2019, **48**, 2422–2457.
- 50 S. Biswas and Y. Negishi, *J. Phys. Chem. Lett.*, 2024, **15**, 947–958.
- 51 H. Hirai, S. Ito, S. Takano, K. Koyasu and T. Tsukuda, *Chem. Sci.*, 2020, **11**, 12233–12248.
- 52 Y. Jin, C. Zhang, X.-Y. Dong, S.-Q. Zang and T. C. Mak, *Chem. Soc. Rev.*, 2021, **50**, 2297–2319.
- 53 S. Biswas, A. K. Das and S. Mandal, *Acc. Chem. Res.*, 2023, **56**, 1838–1849.
- 54 S. Biswas, A. K. Das, S. S. Manna, B. Pathak and S. Mandal, *Chem. Sci.*, 2022, **13**, 11394–11404.
- 55 S. Biswas, A. K. Das, A. C. Reber, S. Biswas, S. Bhandary, V. B. Kamble, S. N. Khanna and S. Mandal, *Nano Lett.*, 2022, **22**, 3721–3727.
- 56 R. K. Gupta, Z. Wang, B. Mohan, C. H. Tung and D. Sun, *Adv. Mater.*, 2024, **36**, 2410054.
- 57 Y.-Z. Huang, R. K. Gupta, G.-G. Luo, Q.-C. Zhang and D. Sun, *Coord. Chem. Rev.*, 2024, **499**, 215508.
- 58 W.-D. Tian, C. Zhang, S. Paul, W.-D. Si, Z. Wang, P.-P. Sun, A. Anoop, C.-H. Tung and D. Sun, *Angew. Chem., Int. Ed.*, 2025, e202421656.
- 59 X. Liu and D. Astruc, *Coord. Chem. Rev.*, 2018, **359**, 112–126.
- 60 Z. Wang, B. Chen and A. L. Rogach, *Nanoscale Horiz.*, 2017, **2**, 135–146.
- 61 S. Maity, D. Bain and A. Patra, *Nanoscale*, 2019, **11**, 22685–22723.
- 62 H. Lin, X. Song, O. J. H. Chai, Q. Yao, H. Yang and J. Xie, *Adv. Mater.*, 2024, **36**, 2401002.
- 63 A. K. Das, S. Biswas, S. S. Manna, B. Pathak and S. Mandal, *Chem. Sci.*, 2022, **13**, 8355–8364.
- 64 S. Biswas, A. Pal, M. K. Jena, S. Hossain, J. Sakai, S. Das, B. Sahoo, B. Pathak and Y. Negishi, *J. Am. Chem. Soc.*, 2024, **146**, 20937–20944.
- 65 R. K. Raju, P. Rodriguez and E. N. Brothers, *Phys. Chem. Chem. Phys.*, 2023, **25**, 11630–11652.
- 66 D. R. Kauffman, D. Alfonso, C. Matranga, H. Qian and R. Jin, *J. Am. Chem. Soc.*, 2012, **134**, 10237–10243.
- 67 M. Zhu, C. M. Aikens, F. J. Hollander, G. C. Schatz and R. Jin, *J. Am. Chem. Soc.*, 2008, **130**, 5883–5885.
- 68 D. R. Kauffman, D. Alfonso, C. Matranga, P. Ohodnicki, X. Deng, R. C. Siva, C. Zeng and R. Jin, *Chem. Sci.*, 2014, **5**, 3151–3157.
- 69 B. Kim, H. Seong, J. T. Song, K. Kwak, H. Song, Y. C. Tan, G. Park, D. Lee and J. Oh, *ACS Energy Lett.*, 2020, **5**, 749–757.
- 70 H. Seong, V. Efremov, G. Park, H. Kim, J. S. Yoo and D. Lee, *Angew. Chem., Int. Ed.*, 2021, **60**, 14563–14570.
- 71 K. Kwak, Q. Tang, M. Kim, D.-E. Jiang and D. Lee, *J. Am. Chem. Soc.*, 2015, **137**, 10833–10840.
- 72 H. Qian, Y. Zhu and R. Jin, *ACS Nano*, 2009, **3**, 3795–3803.
- 73 H. Qian and R. Jin, *Chem. Mater.*, 2011, **23**, 2209–2217.
- 74 S. Li, A. V. Nagarajan, Y. Li, D. R. Kauffman, G. Mpourmpakis and R. Jin, *Nanoscale*, 2021, **13**, 2333–2337.





- 75 J. Wang, F. Xu, Z. Y. Wang, S. Q. Zang and T. C. Mak, *Angew. Chem., Int. Ed.*, 2022, **61**, e202207492.
- 76 S.-F. Yuan, R.-L. He, X.-S. Han, J.-Q. Wang, Z.-J. Guan and Q.-M. Wang, *Angew. Chem., Int. Ed.*, 2021, **60**, 14345–14349.
- 77 M. R. Narouz, K. M. Osten, P. J. Unsworth, R. W. Y. Man, K. Salorinne, S. Takano, R. Tomihara, S. Kaappa, S. Malola, C.-T. Dinh, J. D. Padmos, K. Ayoo, P. J. Garrett, M. Nambo, J. H. Horton, E. H. Sargent, H. Häkkinen, T. Tsukuda and C. M. Crudden, *Nat. Chem.*, 2019, **11**, 419–425.
- 78 S. Li, A. V. Nagarajan, X. Du, Y. Li, Z. Liu, D. R. Kauffman, G. Mpourmpakis and R. Jin, *Angew. Chem., Int. Ed.*, 2022, **61**, e202211771.
- 79 Z. Liu, J. Chen, B. Li, D.-E. Jiang, L. Wang, Q. Yao and J. Xie, *J. Am. Chem. Soc.*, 2024, **146**, 11773–11781.
- 80 S. Zhao, N. Austin, M. Li, Y. Song, S. D. House, S. Bernhard, J. C. Yang, G. Mpourmpakis and R. Jin, *ACS Catal.*, 2018, **8**, 4996–5001.
- 81 V. K. Kulkarni, B. N. Khirak, S. Takano, S. Malola, E. L. Albright, T. I. Levchenko, M. D. Aloisio, C.-T. Dinh, T. Tsukuda, H. Häkkinen and C. M. Crudden, *J. Am. Chem. Soc.*, 2022, **144**, 9000–9006.
- 82 Z.-H. Gao, K. Wei, T. Wu, J. Dong, D.-E. Jiang, S. Sun and L.-S. Wang, *J. Am. Chem. Soc.*, 2022, **144**, 5258–5262.
- 83 S. M. Han, M. Park, J. Kim and D. Lee, *Angew. Chem., Int. Ed.*, 2024, **63**, e202404387.
- 84 Z. Wang, T. Li, Q. Wang, A. Guan, N. Cao, A. M. Al-Enizi, L. Zhang, L. Qian and G. Zheng, *J. Power Sources*, 2020, **476**, 228705.
- 85 H. Seong, M. Choi, S. Park, H.-W. Kim, J. Kim, W. Kim, J. S. Yoo and D. Lee, *ACS Energy Lett.*, 2022, **7**, 4177–4184.
- 86 C. P. Joshi, M. S. Bootharaju, M. J. Alhilaly and O. M. Bakr, *J. Am. Chem. Soc.*, 2015, **137**, 11578–11581.
- 87 L. Qin, F. Sun, X. Ma, G. Ma, Y. Tang, L. Wang, Q. Tang, R. Jin and Z. Tang, *Angew. Chem., Int. Ed.*, 2021, **60**, 26136–26141.
- 88 L. Chen, F. Sun, Q. Shen, L. Qin, Y. Liu, L. Qiao, Q. Tang, L. Wang and Z. Tang, *Nano Res.*, 2022, **15**, 8908–8913.
- 89 Y. Chen, X. Zhou, X. Liu, Z. Tang, L. Wang and Q. Tang, *J. Am. Chem. Soc.*, 2025, **147**, 2699–2713.
- 90 S. Biswas, S. Das and Y. Negishi, *Nanoscale Horiz.*, 2023, **8**, 1509–1522.
- 91 J. Huang, X. Zhang, J. Yang, J. Yu, Q. Chen and L. Peng, *Adv. Sci.*, 2024, **11**, 2309865.
- 92 Y. Ma, M. Sun, H. Xu, Q. Zhang, J. Lv, W. Guo, F. Hao, W. Cui, Y. Wang, J. Yin, H. Wen, P. Lu, G. Wang, J. Zhou, J. Yu, C. Ye, L. Gan, D. Zhang, S. Chu, L. Gu, M. Shao, B. Huang and Z. Fan, *Adv. Mater.*, 2024, 2402979.
- 93 J. Wang, M. Sun, H. Xu, F. Hao, Q. Wa, J. Su, J. Zhou, Y. Wang, J. Yu, P. Zhang, R. Ye, S. Chu, B. Huang, M. Shao and Z. Fan, *ACS Nano*, 2024, **18**, 7192–7203.
- 94 L. Guo, J. Zhou, F. Liu, X. Meng, Y. Ma, F. Hao, Y. Xiong and Z. Fan, *ACS Nano*, 2024, **18**, 9823–9851.
- 95 Y. Ma, J. Yu, M. Sun, B. Chen, X. Zhou, C. Ye, Z. Guan, W. Guo, G. Wang, S. Lu, D. Xia, Y. Wang, Z. He, L. Zheng, Q. Yun, L. Wang, J. Zhou, P. Lu, J. Yin, Y. Zhao, Z. Luo, L. Zhai, L. Liao, Z. Zhu, R. Ye, Y. Chen, Y. Lu, S. Xi, B. Huang, C.-S. Lee and Z. Fan, *Adv. Mater.*, 2022, **34**, 2110607.
- 96 S. Biswas and Y. Negishi, *Dalton Trans.*, 2024, **53**, 9657–9663.
- 97 A. Pal, S. Biswas, B. Sahoo and Y. Negishi, *Synlett*, 2025, DOI: [10.1055/a-2504-3530](https://doi.org/10.1055/a-2504-3530).
- 98 M. Kamiyama, Y. Shingyouchi, R. Sarma, M. Ghosh, T. Kawawaki, S. Biswas and Y. Negishi, *Chem. Commun.*, 2025, **61**, 1048–1062.
- 99 R. S. Dhayal, J.-H. Liao, S. Kahlal, X. Wang, Y.-C. Liu, M.-H. Chiang, W. E. van Zyl, J.-Y. Saillard and C. W. Liu, *Chem. – Eur. J.*, 2015, **21**, 8369–8374.
- 100 Q. Tang, Y. Lee, D.-Y. Li, W. Choi, C. Liu, D. Lee and D.-E. Jiang, *J. Am. Chem. Soc.*, 2017, **139**, 9728–9736.
- 101 F. Li and Q. Tang, *J. Catal.*, 2020, **387**, 95–101.
- 102 S. Li, X. Yan, J. Tang, D. Cao, X. Sun, G. Tian, X. Tang, H. Guo, Q. Wu, J. Sun, J. He and H. Shen, *Chem. Mater.*, 2023, **35**, 6123–6132.
- 103 Y. Shingyouchi, M. Ogami, S. Biswas, T. Tanaka, M. Kamiyama, K. Ikeda, S. Hossain, Y. Yoshigoe, D. J. Osborn, G. F. Metha, T. Kawawaki and Y. Negishi, *Small*, 2024, 2409910.
- 104 S. Biswas, Y. Shingyouchi, M. Kamiyama, M. K. Jana, M. Ogami, T. Kawawaki, B. Pathak and Y. Negishi, *Small*, 2025, 2500302.
- 105 L. Zhang, X.-X. Li, Z.-L. Lang, Y. Liu, J. Liu, L. Yuan, W.-Y. Lu, Y.-S. Xia, L.-Z. Dong and D.-Q. Yuan, *J. Am. Chem. Soc.*, 2021, **143**, 3808–3816.
- 106 S. Biswas, T. Tanaka, H. Song, M. Ogami, Y. Shingyouchi, S. Hossain, M. Kamiyama, T. Kosaka, R. Nakatani, Y. Niihori, S. Das, T. Kawawaki, D.-E. Jiang and Y. Negishi, *Small Sci.*, 2025, **5**, 2400465.
- 107 Q.-J. Wu, D.-H. Si, P.-P. Sun, Y.-L. Dong, S. Zheng, Q. Chen, S.-H. Ye, D. Sun, R. Cao and Y.-B. Huang, *Angew. Chem., Int. Ed.*, 2023, **62**, e202306822.
- 108 L. J. Liu, Z. Y. Wang, Z. Y. Wang, R. Wang, S. Q. Zang and T. C. Mak, *Angew. Chem., Int. Ed.*, 2022, **61**, e202205626.
- 109 W.-L. Mu, L. Li, X.-Z. Cong, X. Chen, P. Xia, Q. Liu, L. Wang, J. Yan and C. Liu, *J. Am. Chem. Soc.*, 2024, **146**, 28131–28140.
- 110 A. Guan, C. Yang, Q. Wang, L. Qian, J. Cao, L. Zhang, L. Wu and G. Zheng, *ACS Sustainable Chem. Eng.*, 2021, **9**, 13536–13544.
- 111 M. Salehi, H. Al-Mahayni, A. Farzi, M. McKee, S. Kaviani, E. Pajootan, R. Lin, N. Kornienko and A. Seifitokaldani, *Appl. Catal., B*, 2024, **353**, 124061.
- 112 P. Iyengar, J. Huang, G. L. De Gregorio, C. Gadiyar and R. Buonsanti, *Chem. Commun.*, 2019, **55**, 8796–8799.
- 113 D. Cheng, Z.-J. Zhao, G. Zhang, P. Yang, L. Li, H. Gao, S. Liu, X. Chang, S. Chen, T. Wang, G. A. Ozin, Z. Liu and J. Gong, *Nat. Commun.*, 2021, **12**, 395.
- 114 F. Chang, M. Xiao, R. Miao, Y. Liu, M. Ren, Z. Jia, D. Han, Y. Yuan, Z. Bai and L. Yang, *Electrochem. Energy Rev.*, 2022, **5**, 4.
- 115 J. He, N. J. Johnson, A. Huang and C. P. Berlinguette, *ChemSusChem*, 2018, **11**, 48–57.
- 116 L. Liu, H. Akhoundzadeh, M. Li and H. Huang, *Small Methods*, 2023, **7**, 2300482.
- 117 X. Kang, Y. Li, M. Zhu and R. Jin, *Chem. Soc. Rev.*, 2020, **49**, 6443–6514.



- 118 S. Li, D. Alfonso, A. V. Nagarajan, S. D. House, J. C. Yang, D. R. Kauffman, G. Mpourmpakis and R. Jin, *ACS Catal.*, 2020, **10**, 12011–12016.
- 119 S. Zhuang, D. Chen, L. Liao, Y. Zhao, N. Xia, W. Zhang, C. Wang, J. Yang and Z. Wu, *Angew. Chem., Int. Ed.*, 2020, **59**, 3073–3077.
- 120 S. Li, A. V. Nagarajan, D. R. Alfonso, M. Sun, D. R. Kauffman, G. Mpourmpakis and R. Jin, *Angew. Chem., Int. Ed.*, 2021, **60**, 6351–6356.
- 121 Y. Sun, X. Liu, K. Xiao, Y. Zhu and M. Chen, *ACS Catal.*, 2021, **11**, 11551–11560.
- 122 X. Ma, F. Sun, L. Qin, Y. Liu, X. Kang, L. Wang, D.-E. Jiang, Q. Tang and Z. Tang, *Chem. Sci.*, 2022, **13**, 10149–10158.
- 123 G. Deng, J. Kim, M. S. Bootharaju, F. Sun, K. Lee, Q. Tang, Y. J. Hwang and T. Hyeon, *J. Am. Chem. Soc.*, 2023, **145**, 3401–3407.
- 124 G. Deng, H. Yun, M. S. Bootharaju, F. Sun, K. Lee, X. Liu, S. Yoo, Q. Tang, Y. J. Hwang and T. Hyeon, *J. Am. Chem. Soc.*, 2023, **145**, 27407–27414.
- 125 S. Su, Y. Zhou, L. Xiong, S. Jin, Y. Du and M. Zhu, *Angew. Chem., Int. Ed.*, 2024, **63**, e202404629.
- 126 L. Shi, H. Wu, W. Xu, W. Fu, X. Wang, Z. Gu, X. Zhang, J. Chen, Y. Ma and J. Zhao, *Sci. Chin. Mater.*, 2024, **67**, 3602–3608.

